Gravitino Dark Matter with Entropy Production constrained by Big Bang Nucleosynthesis

Håkon Vinje Høines

Advisor: Jörn Kersten

A thesis presented for the degree of

Master of Science

December 16, 2016

UNIVERSITY OF BERGEN

Faculty of Mathematics and Natural Sciences

University of Bergen

Norway

Abstract

We are looking at a gravitino dark matter scenario with a general neutralino next-to-lightest supersymmetric particle. We are considering the primary decay channels of the neutralino, and we define the supersymmetric parameters in the high energy regime. We compare with the bounds enforced by big bang nucleosynthesis, and we compare with models defined in the low energy regime. Then, we introduce early universe entropy production and see how the available parameter space is affected. Finally, we discuss the limits on the gravitino mass and how they coincide with the current dark matter observations.

Contents

Chapter 1

Introduction

The extended Standard Model (SM) with neutrino masses is an accurate and well functioning model of the real world, and has had great success up to the $\sim$ TeV energy scale. But at higher scales approaching the Grand Unified Theory (GUT) scale $M_p = 2.435 \times 10^{18}$ GeV, SM breaks down, as quantum gravitational effects become non-negligible. This is a problem because the scalar Higgs mass receives quantum corrections from every particle that couples to the Higgs field, proportional to the coupling strength times the scale where new physics is expected to appear. That is

$$\Delta m_H^2 \propto - \left| \lambda_f \right|^2 \Lambda_{UV}^2, \qquad \Delta m_H^2 \propto \lambda_S \Lambda_{UV}^2 \tag{1.1}$$

for fermions and scalars respectively. For the top quark with $\lambda_f \approx 1$, this correction is about 30 orders of magnitude larger than the required value $m_H^2 \sim -(100\text{GeV})^2$ at the $\Lambda_{UV} \sim M_p$ scale [1]. This is known as the "hierarchy problem".

Supersymmetry (SUSY) is one solution to the hierarchy problem. SUSY introduces one new particle for each SM particle with the exact opposite contribution to the quantum corrections to the Higgs as the SM particle, and thus the SM-SUSY particle pair will cancel each others contribution. A secondary effect of this solution is that we have a whole new range of particles to explore. We find that some of these new particles have the desired

properties of being uncharged and weakly interacting, and are therefore good candidates for dark matter. We know that dark matter exists, as we have observed its gravitational effects on the rotation curves of galaxies and the curvature of space. We also know that the dark matter can not interact electromagnetically, as these interactions are easy to observe, which is why the uncharged and weakly interacting nature of these SUSY particles is desirable. Further, we can use current data from the Large Hadron Collider (LHC) to restrict the masses of the new SUSY particles from below, as they remain undetected. The abundance of dark matter has also been found using the cosmic microwave background radiation data from the Wilkinson Microwave Anisotropy Probe (WMAP) to be $\Omega_{DM} \approx 0.1$ [2], which we will come back to later.

In this thesis, we will investigate the implications of letting one of these candidates in SUSY be the dark matter particle. We will consider the SUSY particle gravitino as the dark matter, explore how the current abundance of dark matter came to be, and then exhaust the parameter space to find parameter tuples that fall within the allowed range enforced by the constraints extracted from observational data.

In the next chapter, we will describe some of the standard cosmology. We will describe how the universe evolve with time, how early events affect current observational data, and how the light elements in the universe is created. In chapter 3, we will roughly introduce the mathematics of the supersymmetric theory, all the SUSY particles, and describe in detail the most important of them related to dark matter production. In chapter 4, we will describe the primary decay channels into dark matter, and the associated lifetime calculations. In chapter 5, we will produce plots built upon all the previous chapters, where we plot the parameter space with the given constraints, and analyse how the input parameters affect the validity of the output with respect to the observational constraints.

Chapter 2

Evolution of the Universe

The discovery of General Relativity by Einstein lead to more accurate models of the large scale dynamics of the universe. The most popular model, and the one we refer to as 'Standard Cosmology', is the Friedmann-Robertson-Walker metric, or the FRW metric. This metric is an exact solution of the Einstein field equations describing an homogeneous, isotropic, expanding and/or contracting universe

$$ds^2 = c^2dt^2 - a^2 \left[\frac{dr^2}{1 - kr^2} + r^2(d\theta^2 + sin^2\theta d\phi^2) \right] \qquad (2.1)$$

where t, r, θ, and ϕ are the space-time coordinates, s is the proper length, c is the speed of light, $a \equiv a(t)$ is the scale factor, which is related to the expansion of the universe, and k is related to the curvature of the universe, with $k = 0$ corresponding to a flat universe.

Inserting the FRW metric back into the field equations for General Relativity, using a diagonal stress-energy tensor $T^\mu_\nu = \text{diag}(\rho, -p, -p, -p)$ and gravitational constant G, we can extract a simpler expression describing the expansion of the universe

$$\frac{k}{\dot{a}^2} = \frac{8\pi G\rho a^2}{3\dot{a}^2} - 1 \qquad (2.2)$$

Using the Hubble parameter, $H \equiv \dot{a}/a$ (Where today's value is $H_0 = 100h$

km s^{-1} Mpc^{-1} with uncertainty h), we can rewrite this expression as

$$\frac{k}{H^2 a^2} = \frac{8\pi G\rho}{H^2} - 1 \equiv \frac{\rho}{\rho_C} - 1 \equiv \Omega - 1 \tag{2.3}$$

with Ω, the relic density, defined as the energy density divided by some critical energy density. This is known as the Friedmann Equation.

The relic density is an interesting property to explore, as it is related to both the curvature and the energy density of the universe. These quantities can be expanded to different particle species' individual contributions

$$\Omega = \sum_i \Omega_i = \sum_i \frac{\rho_i}{\rho_C} = \frac{\rho}{\rho_C} \tag{2.4}$$

It is useful to note that the individual species' relic density is related to the total energy density of the given species, and by extension, the number density of the given species, and it is therefore easy to see that interaction resonances will affect the relic density severely.

2.1 Decaying Particles and Entropy Production in the Early Universe

Consider a non-relativistic, long lived particle ϕ, in a radiation dominated universe. From energy conservation, we know that the energy density for a non-relativistic particle, ρ_{mat}, in a comoving volume in an expanding universe is inversely proportional to a^3. For relativistic particles, we also have another factor a from the redshifting of the wavelength, and therefore have energy density, ρ_{rad}, inversely proportional to a^4. Hence, if ϕ is sufficiently long lived, the energy density of ϕ will come to dominate the universe as time increases, since $\rho_{mat}/\rho_{rad} \propto a$.

The matter dominated period caused by the long lived ϕ will last until the ϕ decays have produced enough radiation to make the universe radiation dominated again. As the temperature will decrease more slowly in a matter dominated universe compared to a radiation dominated universe [3], we end

8

up with a higher temperature $T(t \gg \tau_\phi)$ compared to if ϕ decayed before it could dominate the energy density of the universe.

As the entropy density in a comoving volume is $s \propto T^3$, we see that a difference in temperature leads to an increased entropy density in the case where the ϕ is long lived, compared to if it decayed before it could dominate the total energy density of the universe. Therefore, as total entropy in the universe is usually conserved, we can define the dilution factor as the change in total entropy as a result of the entropy produced by the decaying particles as

$$\Delta \equiv \frac{S_{final}}{S_{initial}} \tag{2.5}$$

This change in entropy can also be shown to have an effect on the relic density of a particle, more specifically, the current relic density of a particle with entropy production (Ω^Δ) is proportional to the current relic density without entropy production (Ω)

$$\Omega^\Delta = \frac{1}{\Delta}\Omega \tag{2.6}$$

We see that this affects all particles that froze out (i.e. their interaction rate becomes smaller than the Hubble parameter) before ϕ decayed, as they do not longer interact with the thermal heat bath. Therefore, their relic density will be diluted compared to if they froze out after ϕ decayed. In standard cosmology, the dilution factor is taken to be $\Delta = 1$. Later we will explore the implications when $\Delta > 1$.

2.2   Big Bang Nucleosynthesis

The synthesis of light elements in the early universe is known as Big Bang Nucleosynthesis (BBN), and is a reliable probe into the early universe [4]. Based on SM and without introducing any free parameters [5], BBN predicts the abundance of the light elements D, ^{3}He, ^{4}He, and ^{7}Li in the universe. These values are essentially constant after $t \sim 3$ min, but are affected by the stellar production of the heavier elements. Therefore, when measuring these

abundances, we seek out areas with the smallest degree of heavy elements as possible, to measure the light element abundances closer to how they were right after BBN.

Given the initial conditions for BBN, that is $T \gg 1$ MeV and $t \ll 1$ sec, there is a balance between protons and neutrons maintained by the weak interactions related to β-decay [6]. This epoch is dominated by the relativistic γ, $e^{\pm}$, and the 3 neutrino species, as the nucleons are too heavy to be relativistic. Shortly before the universe cools down to $T \sim 1$ MeV ($t \sim 1$ sec), the neutrinos decouple from the heat bath, and a little later ($T \sim m_e/3$), the $e^{\pm}$ pairs annihilate, transferring their entropy to the photons, raising the photon temperature relative to that of the neutrinos. At about the same time, the weak interactions which are maintaining the proton-neutron equilibrium freezes out, with a proton-neutron ratio of about 6. When the temperature reaches $T \sim 0.3 - 0.1$ MeV ($t \sim 1 - 3$ min), the proton-neutron ratio has reached about 7 from some occasional weak interactions.

Earlier, the abundances of the light elements were non-zero but negligible, but in this epoch between $T \sim 0.3$ MeV and $T \sim 0.1$ MeV, the temperature is low enough that light nuclei may form without being instantly ripped apart. This can easily be shown using Boltzmann statistics. We can calculate the Nuclear Statistical Equilibrium (NSE) number density, n_A, for a non-relativistic nucleus A with mass m_A ($m_A \gg T$), g_A degrees of freedom, and chemical potential μ_A

$$n_A = g_A \left(\frac{m_A T}{2\pi} \right)^{3/2} \exp \left(\frac{\mu_A - m_A}{T} \right) \tag{2.7}$$

In the case of chemical equilibrium, we can rewrite this expression in terms of the proton and neutron densities, and B_A, the binding energy of the nucleus $A(Z)$ with A nucleons and Z protons, using the nucleon mass $m_N = m_n = m_p = m_A/A$, as the differences of these masses are not important to us, as such

$$n_A = g_A A^{3/2} 2^{-A} \left(\frac{2\pi}{m_N T} \right)^{3(A-1)/2} n_p^Z n_n^{A-Z} \exp(B_A/T) \tag{2.8}$$

10

Multiplying by A and dividing by $n_N = n_n + n_p + \sum_{species}(An_A)$, we obtain the fraction of baryons, out of all baryons, that are occupied in $A(Z)$ states

$$X_A \equiv \frac{n_A A}{n_N} = g_A[\zeta(3)^{A-1}\pi^{(1-A)/2}2^{(3A-5)/2}]A^{5/2}(T/m_N)^{3(A-1)/2}$$
$$\times \eta^{A-1}X_p^Z X_n^{A-Z}\exp(B_A/T) \tag{2.9}$$

where $\zeta(3) = 1.20206...$ is the Riemann-Zeta function of 3, and $\eta \equiv n_N/n_\gamma$ the nucleon-to-photon ratio. Here we can easily see that for $T > B_A$, the fraction goes to zero exponentially, verifying the statement in the beginning of this paragraph.

At the beginning of the epoch when nuclei start to form, the rates of the ^{4}He producing processes are not high enough for ^{4}He to reach NSE. The reasons for this are firstly, that the abundances of D, ^{3}He, and ^{3}H, even though they are reaching NSE, are still quite small, $X_i < 10^{-12}$. Secondly, the coulomb suppression is starting to become significant. When the abundances of D, ^{3}He, and ^{3}H become large enough for ^{4}He to reach NSE at $T \simeq 0.1$ MeV, the coulomb suppression has become very significant, and only a tiny amount of ^{7}Li can be synthesised from ^{4}He. This explains why there will be issues with BBN predictions if a large amount of particles decay during or after BBN, as the ratios would be significantly different if this were the case.

The degree of how much the BBN predictions are altered is naturally dependent on the available decay channels of the long lived particle species, as different resulting particles can bind themselves to the light nuclei and change the required energy for more nucleons to bind to the nucleus, thereby changing the resulting abundance. These resultant decay products can also interact with the surrounding nuclei in the thermalization process, and thereby splitting them into their constituent nucleons as a way to dissipate energy [7]. Hence, we see that for an abundance of a given particle, BBN restricts the allowed lifetime of the particle as to not interfere with the synthesis of the light elements. These constraints are of course more severe the higher the hadronic branching ratio of the particle is, as hadrons are more involved in the formation of nuclei. Therefore, we have an upper bound on the allowed

relic density for a particle with a given mass, depending on the available decay channels.

By using observational data, lower bounds on the abundance of light elements can be determined. If we explore how the given parameters in (2.9) changes the resulting abundance of the light elements, we can determine the allowed parameter space such that the lower bounds still hold. Following this argument, we can calculate how the decay of a particle would change these parameters, and thus apply the same constraints on the properties of the decaying particle. This has been done for decaying relic neutral particles in [7], and these are the bounds we will consider later on.

Chapter 3

Supersymmetry

SUSY is one way to solve the hierarchy problem. For each SM particle, SUSY introduces a new particle with the spin offset by one half. Thus, each SM boson has a fermionic SUSY partner, and each SM fermion has a bosonic SUSY partner. This is a valid solution to the hierarchy problem as the relative minus sign between bosonic and fermionic contribution makes the terms cancel each other out.

Had SUSY been unbroken, we would have found the supersymmetric particles with the exact same masses as their SM partners, which we have not, thus we know, that SUSY is a broken symmetry. To make sure that SUSY still is a valid solution to the hierarchy problem, we have to demand that the supersymmetric coupling strength is exactly opposite to the SM coupling strength, e.g. for the stop-top superpair using the notation in [1]

$$\Delta m_H \propto (\lambda_S - |\lambda_f|^2)\Lambda_{UV} = 0 \tag{3.1}$$

thus we have to break SUSY softly. Therefore, we can write the Lagrangian as

$$\mathcal{L} = \mathcal{L}_{SUSY} + \mathcal{L}_{soft} \tag{3.2}$$

where $\mathcal{L}_{SUSY}$ contains the gauge and Yukawa interactions, and $\mathcal{L}_{soft}$ contains the mass terms and coupling parameters with positive dimensions. We can

express the SUSY Lagrangian as a combination of a chiral contribution and a gauge contribution, with the chiral part given as

$$\mathcal{L}_{SUSY}^{chiral} = -D^\mu \phi^{*i} D_\mu \phi_i + i\psi^{\dagger i}\bar{\sigma}^\mu D_\mu \psi_i - \frac{1}{2}(W^{ij}\psi_i \psi_j + W_{ij}^* \psi^{\dagger i}\psi^{\dagger j}) - W^i W_i^* \tag{3.3}$$

where ϕ^i are the scalar fields, ψ^i are the fermion fields, D_μ is the covariant derivative, σ^i are given by

$$\sigma^0 = \bar{\sigma}^0 = \begin{pmatrix} 1 & 0 \\ 0 & 1 \end{pmatrix}, \qquad \sigma^1 = -\bar{\sigma}^1 = \begin{pmatrix} 0 & 1 \\ 1 & 0 \end{pmatrix},$$
$$\sigma^2 = -\bar{\sigma}^2 = \begin{pmatrix} 0 & -i \\ i & 0 \end{pmatrix}, \quad \sigma^3 = -\bar{\sigma}^3 = \begin{pmatrix} 1 & 0 \\ 0 & -1 \end{pmatrix}, \tag{3.4}$$

and the W^i and W^{ij} are given from the superpotential W as such

$$W^i = \frac{\delta W}{\delta \phi_i}, \qquad W^{ij} = \frac{\delta^2}{\delta \phi_i \delta \phi_j} W \tag{3.5}$$

The gauge part of the Lagrangian can be expressed as

$$\mathcal{L}_{SUSY}^{gauge} = \sum_\Lambda \left[-\frac{1}{4}F_{\mu\nu}^a F^{\mu\nu a} + i\lambda^{\dagger a}\bar{\sigma}^\mu D_\mu \lambda^a \right]_\Lambda \tag{3.6}$$

where Λ runs over all the gauge groups, a runs over the adjoint representation of the gauge group ($a = 1, ..., 8$ for SU(3)$_C$, $a = 1, ..., 3$ for SU(2)$_L$, and $a = 1$ for U(1)$_Y$), λ_a are the fermionic gauginos, $F_{\mu\nu}^a$ is given by

$$F_{\mu\nu}^a = \partial_\mu A_\nu^a - \partial_\nu A_\mu^a + gf^{abc}A_\mu^b A_\nu^c \tag{3.7}$$

where g is the gauge coupling strength, and the covariant derivatives are given by

$$D_\mu \phi_i = \partial_\mu \phi_i - \sum_\Lambda \left[ig A_\mu^a (T^a \phi)_i \right]_\Lambda$$
$$D_\mu \phi^{*i} = \partial_\mu \phi^{*i} + \sum_\Lambda \left[ig A_\mu^a (T^a \phi^*)_i \right]_\Lambda$$
$$D_\mu \psi_i = \partial_\mu \psi_i - \sum_\Lambda \left[ig A_\mu^a (T^a \psi)_i \right]_\Lambda \tag{3.8}$$
$$D_\mu \lambda^a = \partial_\mu \lambda^a + \sum_\Lambda \left[gf^{abc} A_\mu^b \lambda^c \right]_\Lambda$$

Here, A_μ^a are the gauge bosons, f^{abc} are the antisymmetric structure constants that define the gauge group, and T^a are the generators of the gauge group or 0 depending on if there is a coupling to the gauge group or not. Now, we can combine this into the general SUSY Lagrangian

$$\mathcal{L}_{SUSY} = \mathcal{L}_{SUSY}^{chiral} + \mathcal{L}_{SUSY}^{gauge}$$
$$- \sum_\Lambda \left[\frac{1}{2}g^2(\phi^{*i}T^a\phi_i)^2 + \sqrt{2}g(\phi^{*i}T^a\psi_i)\lambda^a + \sqrt{2}g\lambda^{\dagger a}(\psi^{\dagger i}T^a\phi_i) \right]_\Lambda$$

(3.9)

Here, we see that the last 2 terms give us coupling between the gauginos and the particle pairs in a supermulitplet. The soft part of the Lagrangian for a general SUSY model can be written as such

$$\mathcal{L}_{soft} = -\left(\frac{1}{2}M_a\lambda^a\lambda^a + \frac{1}{6}a^{ijk}\phi_i\phi_j\phi_k + \frac{1}{2}b^{ij}\phi_i\phi_j + t^i\phi_i + \text{h.c.} \right) - (m^2)_j^i\phi^{*j}\phi_i$$
$$- \left(\frac{1}{2}c_i^{jk}\phi^{*i}\phi_j\phi_k + \text{h.c.} \right)$$

(3.10)

where h.c. denotes the hermitian conjugate. Here, the first line has been rigorously proven that will not introduce any quadratic divergence in the quantum corrections to scalar masses. The second line is not so certain as some combinations will break the soft requirement and introduce divergences, and is therefore often neglected.

In the Minimal Supersymmetric Standard Model (MSSM) using the symbols given in Table 3.1, the superpotential looks like

$$W^{MSSM} = \widetilde{u}\boldsymbol{y_u}\widetilde{Q}H_u' - \widetilde{d}\boldsymbol{y_d}\widetilde{Q}H_d' - \widetilde{e}\boldsymbol{y_e}\widetilde{L}H_d' + \mu H_u'H_d' \qquad (3.11)$$

where the first three terms are the Yukawa couplings and the last term is related to the mass of the Higgses. $\mathcal{L}_{soft}$ in MSSM is expressed as

$$\mathcal{L}_{soft}^{MSSM} = -\frac{1}{2}(M_3\widetilde{g}\widetilde{g} + M_2\widetilde{W}\widetilde{W} + M_1\widetilde{B}\widetilde{B} + \text{h.c.})$$
$$- (\widetilde{u}\boldsymbol{a_u}\widetilde{Q}H_u' - \widetilde{d}\boldsymbol{a_d}\widetilde{Q}H_d' - \widetilde{e}\boldsymbol{a_e}\widetilde{L}H_d' + \text{h.c.})$$
$$- \widetilde{Q}^\dagger\boldsymbol{m_Q^2}\widetilde{Q} - \widetilde{L}^\dagger\boldsymbol{m_L^2}\widetilde{L} - \widetilde{u}\boldsymbol{m_{\widetilde{u}}^2}\widetilde{u}^\dagger - \widetilde{d}\boldsymbol{m_{\widetilde{d}}^2}\widetilde{d}^\dagger - \widetilde{e}\boldsymbol{m_{\widetilde{e}}^2}\widetilde{e}^\dagger$$
$$- m_{H_u}^2 H_u'^* H_u' - m_{H_d}^2 H_d'^* H_d' - (bH_u'H_d' + \text{h.c.})$$

(3.12)

Name		Spin 0	Spin 1/2	$SU(3)_C, SU(2)_L, U(1)_Y$
squarks, quarks	Q	$(\widetilde{u}_L \quad \widetilde{d}_L)$	$(u_L \quad d_L)$	$(\mathbf{3}, \mathbf{2}, \frac{1}{6})$
(3 families)	$\bar{u}$	$\widetilde{u}_R^*$	$u_R^\dagger$	$(\bar{\mathbf{3}}, \mathbf{1}, -\frac{2}{3})$
	$\bar{d}$	$\widetilde{d}_R^*$	$d_R^\dagger$	$(\bar{\mathbf{3}}, \mathbf{1}, \frac{1}{3})$
sleptons, leptons	L	$(\widetilde{\nu} \quad \widetilde{e}_L)$	$(\nu \quad e_L)$	$(\mathbf{1}, \mathbf{2}, -\frac{1}{2})$
(3 families)	$\bar{e}$	$\widetilde{e}_R^*$	$e_R^\dagger$	$(\mathbf{1}, \mathbf{1}, 1)$
Higgses, Higgsinos	H_u	$(H_u^+ \quad H_u^0)$	$(\widetilde{H}_u^+ \quad \widetilde{H}_u^0)$	$(\mathbf{1}, \mathbf{2}, \frac{1}{2})$
	H_d	$(H_d^0 \quad H_d^-)$	$(\widetilde{H}_d^0 \quad \widetilde{H}_d^-)$	$(\mathbf{1}, \mathbf{2}, -\frac{1}{2})$
		Spin 1/2	Spin 1	
gluino, gluon		$\widetilde{g}$	g	$(\mathbf{8}, \mathbf{1}, 0)$
winos, W bosons		$\widetilde{W}^\pm, \quad \widetilde{W}^0$	$W^\pm, \quad W^0$	$(\mathbf{1}, \mathbf{3}, 0)$
bino, B boson		$\widetilde{B}^0$	B^0	$(\mathbf{1}, \mathbf{1}, 0)$

Table 3.1: The chiral (top) and gauge (bottom) supermultiplets in MSSM. The spin 0 fields are complex scalars and the spin 1/2 chiral fields are left-handed 2 component Weyl spinors. We also have to introduce a second Higgs doublet as the superpotential has to be analytic and therefore can not contain conjugates. The SUSY element in a chiral supermultiplet will be referred to as the symbol with a tilde above, and the SM element will be referred to with an apostrophe (example: $\widetilde{Q} = (\widetilde{u}_L \quad \widetilde{d}_L)$ and $Q' = (u_L \quad d_L)$).

In the $\mathcal{L}_{soft}^{MSSM}$ expression, M_1, M_2, and M_3 are the bino, wino, and gluino mass terms respectively. The second line contains the scalar couplings to the Higgs fields, the third line contains the scalar mass terms, and the final line describes the Higgs masses.

From the soft Lagrangian, we can see that there are many more parameters than in SM, which is not the case for the SUSY-preserving part of the Lagrangian [1, 8]. There are as much as 105 free masses, phases, and mixing angles that can not be rotated away, which means that the breaking of SUSY introduces a large amount of arbitrariness to the SUSY Lagrangian. Therefore, at high energy scale $\sim M_p$, it is usual to assume that there is some unification of the parameters, such as making the scalar couplings propor-

tional to the corresponding Yukawa coupling matrix

$$\boldsymbol{a_u} = A_{u0}\boldsymbol{y_u}, \quad \boldsymbol{a_d} = A_{d0}\boldsymbol{y_d}, \quad \boldsymbol{a_e} = A_{e0}\boldsymbol{y_e} \tag{3.13}$$

and the masses proportional to the 3×3 identity matrix

$$\boldsymbol{m_Q^2} = m_Q^2\boldsymbol{1}, \quad \boldsymbol{m_{\bar{u}}^2} = m_{\bar{u}}^2\boldsymbol{1}, \quad \boldsymbol{m_{\bar{d}}^2} = m_{\bar{d}}^2\boldsymbol{1}, \quad \boldsymbol{m_L^2} = m_L^2\boldsymbol{1}, \quad \boldsymbol{m_{\bar{e}}^2} = m_{\bar{e}}^2\boldsymbol{1} \tag{3.14}$$

and lastly, we will assume that no new complex phases are introduced, i.e. the parameters are real. Thus, we can see that besides the SM parameters and Yukawa couplings, there are 3 real gaugino masses, 5 real slepton and squark masses squared, 3 real scalar coupling parameters, and 4 Higgs mass parameters in this idealized form of MSSM.

If we want to extract physical predictions given a set of input parameters at a given energy scale, we have to evolve the parameters using their renormalization group equations, and thus enforce that the loop expansions do not make the observables diverge at different energy scales. The one-loop equations for the gaugino mass parameters are as follows

$$\frac{d}{dt}M_a = \frac{1}{8\pi^2}b_a g_a^2 M_a \tag{3.15}$$

where $b_a = (33/5, 1, -3)$, g_a are the gauge coupling strengths, and $t = \ln(Q/Q_0)$ where Q is the normalization scale and Q_0 is a reference scale. The result of this is that the quantity M_a/g_a^2 is constant with respect to energy scale, and since g_a unify at the M_p scale, it is usual to assume that the mass parameters also unify, that is

$$\frac{M_1}{g_1^2} = \frac{M_2}{g_2^2} = \frac{M_3}{g_3^2} = \frac{m_{1/2}}{g_p^2} \tag{3.16}$$

In this thesis however, we will not assume the unification of the mass parameters. We will consider them as independent parameters instead.

In the case of the two first families of squark and slepton masses, the one loop equations are given as

$$16\pi^2\frac{d}{dt}m_{\phi i}^2 = -\sum_a 8C_a(i)g_a^2|M_a|^2 + \frac{6}{5}Y_i g_1^2 \text{Tr}(Y_j m_{\phi j}^2) \tag{3.17}$$

where $C_a(i)$ is a constant dependent on the gauge group and particle, Y_i is the hypercharge, and j runs over all the scalars in Table 3.1. An important feature of this equation is that the right hand side contains the gaugino mass parameters, and the scalar masses are therefore dependent on the evolution of those as well. Note that such equations exists for the third family and other parameters as well and are implicitly included when referring to the aforementioned renormalization group equations.

3.1   Higgs Sector

In SUSY, we notice that we need 2 Higgs doublets, from the fact that the superpotential is required to be analytic, and are found in Table 3.1 as $H'_u = (H_u^+, H_u^0)^T$ and $H'_d = (H_d^0, H_d^-)^T$. These doublets have 2 complex scalar field each, or 8 real scalar fields combined. When electroweak symmetry breaks, these fields mix to become 3 Nambu-Goldstone bosons G^0 and $G^\pm$, which become longitudinal modes of the Z^0 and $W^\pm$ bosons, and the remaining 5 degrees of freedom become 2 CP-even neutral scalars h and H, the CP-odd neutral scalar A, and the charged scalars $H^\pm$.

As it can be shown that H_u^0 and H_d^0 have non-zero Vacuum Expectation Values (VEV), we use the notation $v_u \equiv \langle H_u^0 \rangle$ and $v_d \equiv \langle H_d^0 \rangle$, and the ratio of these VEVs is defined as $\tan\beta \equiv v_u/v_d$.

We can express H_u^0 and H_d^0 in terms of the mass eigenstates as

$$
\begin{pmatrix} H_u^0 \\ H_d^0 \end{pmatrix} = \begin{pmatrix} v_u \\ v_d \end{pmatrix} + \frac{1}{\sqrt{2}} \begin{pmatrix} c_\alpha & s_\alpha \\ -s_\alpha & c_\alpha \end{pmatrix} \begin{pmatrix} h \\ H \end{pmatrix}
$$
$$
+ \frac{i}{\sqrt{2}} \begin{pmatrix} s_{\beta 0} & c_{\beta 0} \\ -c_{\beta 0} & s_{\beta 0} \end{pmatrix} \begin{pmatrix} G^0 \\ A \end{pmatrix}
\tag{3.18}
$$

where s and c denote sine and cosine of the indexed parameter, α is the mixing angle that diagonalizes the squared mass matrix of the CP-even neutral Higgs bosons [9], and $\beta_0 = \beta$ provided that v_u and v_d minimizes the tree level Higgs potential, which we will assume they do. The mixing angle, α, at tree level

can be determined by

$$\frac{\sin 2\alpha}{\cos 2\beta} = -\left(\frac{m_H^2 + m_h^2}{m_H^2 - m_h^2}\right), \qquad \frac{\tan 2\alpha}{\tan 2\beta} = \left(\frac{m_A^2 + m_Z^2}{m_A^2 - m_Z^2}\right) \qquad (3.19)$$

where m_i is the mass of the indexed particle.

3.2   Gravitino

For supersymmetric models in which we include gravity, also known as supergravity (SUGRA), we include the possibility for a graviton in SM, and therefore require a SUSY partner to the graviton, which is known as the gravitino ($\Psi_{3/2}$), with spin $3/2$ and mass $m_{3/2}$. For unbroken SUSY, the gravitino would be massless and only interact gravitationally, but for broken SUSY, the gravitino absorbs the spin $1/2$ goldstino and its interactions (the particle that emerges from breaking global SUSY) and gains a mass [10].

In this thesis, we will assume that the gravitino is the Lightest Supersymmetric Particle (LSP), because if it is not, the weakly interacting nature of the gravitino would make it decay during or after BBN [11], which would introduce problematic BBN predictions. We can do this because we assume that R-parity is a conserved property within SUSY, that is, SM particles have even parity ($P_R = 1$), and SUSY particles have odd parity ($P_R = -1$). As a result of R-parity conservation, all SUSY particles have to decay into the LSP + SM particles eventually, and the LSP is stable, as is cannot decay into another SUSY particle.

We can also use Boltzmann statistics to calculate the number density of SUSY particles given the interaction rates and masses of the particles [12]. As all heavier SUSY particles decay, R-parity assures that they all decay, where the LSP is an end result of these decays as the LSP is stable. Therefore, we can say that the number density of the LSP is the sum of all SUSY number densities. The relic density of the gravitino before the other SUSY particles decay, the thermally produced gravitinos, can be approximated [13] by

$$\Omega_{3/2} h^2 \simeq 0.2 \left(\frac{100 \text{ GeV}}{m_{3/2}}\right) \left(\frac{m_{\tilde{g}}}{1 \text{ TeV}}\right)^2 \left(\frac{T_R}{10^{10} \text{ GeV}}\right) \qquad (3.20)$$

where $m_{\tilde{g}}$ is the mass of the gluino, and assuming a high reheating temperature T_R which is required for thermal leptogenesis. Here we see that a high gravitino mass is beneficial as this would allow for a wider range of gluino masses without sacrificing the high reheating temperature.

A problem that emerges by choosing the gravitino as the LSP, as we will see in chapter 5, is that when doing the calculations, we find that most of the time the gravitino relic density will be too high compared to the expected dark matter abundance, $\Omega_{3/2} > \Omega_{DM} \approx 0.1$. To solve this problem, we will introduce a non-unity dilution factor to see if early universe entropy production will skew the gravitino relic density in our favour, as seen in (2.6).

3.3   Neutralino

The gauginos $(\widetilde{B}, \widetilde{W}^0)$ and the neutral part of the Higgsinos $(\widetilde{H}_d^0, \widetilde{H}_u^0)$ mix to form 4 mass eigenstates called neutralinos (χ_i^0) from the effect of electroweak symmetry breaking. The neutralinos are ordered from lightest $(i = 1)$ to the heaviest $(i = 4)$, and therefore in this thesis, we will assume that χ_1^0 is the Next-to-Lightest Supersymmetric Particle (NLSP).

In the gauge interaction-eigenstate basis $\psi^0 = (\widetilde{B}, \widetilde{W}^0, \widetilde{H}_d^0, \widetilde{H}_u^0)^T$, the neutralino Lagrangian can be written as such

$$\mathcal{L} = -\frac{1}{2}\psi^{0\dagger}\boldsymbol{M}\psi^0 + \text{h.c.} \tag{3.21}$$

We can easily see from (3.12) that $M_{11} = M_1$ and $M_{22} = M_2$. We also see from the 3rd and 4th term in (3.3) and the last term in (3.11) that $M_{34} = M_{43} = -\mu$. The off-diagonal gaugino-Higgsino mixing is a result of the gaugino-Higgsino-Higgs coupling mentioned in (3.9) and will therefore contain some combination of g and the VEVs of the neutral Higgses. These terms can be rewritten into terms depending on the weak mixing angle, mass

of the Z boson, and $\tan\beta$. Hence, the neutralino mass matrix is given as

$$\boldsymbol{M} = \begin{pmatrix} M_1 & 0 & -s_W c_\beta m_Z & s_W s_\beta m_Z \\ 0 & M_2 & c_W c_\beta m_Z & -c_W s_\beta m_Z \\ -s_W c_\beta m_Z & c_W c_\beta m_Z & 0 & -\mu \\ s_W s_\beta m_Z & -c_W s_\beta m_Z & -\mu & 0 \end{pmatrix} \quad (3.22)$$

where m_Z is the mass of the Z boson, and with s and c as described earlier.

The diagonalization of the mass matrix is done by finding the eigenvalues and the eigenvectors of the mass matrix. If we order the eigenvectors into a 4×4 matrix $\boldsymbol{N}$, we can multiply each side of $\boldsymbol{M}$ by $\boldsymbol{N}^*$ and $\boldsymbol{N}^{-1}$ respectively, and the resulting matrix will have the eigenvalues of the mass matrix in the diagonal. The eigenvectors will therefore describe the mixing of the original interaction basis to acquire the mass eigenstate with mass equal to the corresponding eigenvalue. Doing this, we end up with the neutralino mass matrix

$$\boldsymbol{M}_\chi = \boldsymbol{N}^* \boldsymbol{M} \boldsymbol{N}^{-1} = \begin{pmatrix} m_{\chi_1} & 0 & 0 & 0 \\ 0 & m_{\chi_2} & 0 & 0 \\ 0 & 0 & m_{\chi_3} & 0 \\ 0 & 0 & 0 & m_{\chi_4} \end{pmatrix} \quad (3.23)$$

with the neutralino mass eignestates given as

$$\chi_i^0 = N_{ij}\psi_j^0 \quad (3.24)$$

When we diagonalize the mass matrix, we end up with not all entries being positive so by convention, we choose that m_{χ_3} is negative and we order the neutralinos by the absolute value of the mass. After this diagonalization process, we end up with a Lagrangian as such

$$\mathcal{L} = -\frac{1}{2}\chi^{0\dagger}\boldsymbol{M}_\chi\chi^0 + \text{h.c.} \quad (3.25)$$

As the mixing matrix is unitary, it is easy to see that this is the same Lagrangian as above. Further, we will use m_{χ_1} and m_χ interchangeably, as the other masses are of no interest to us.

21

We define the neutralino relic density, Ω_χ, as the current abundance of neutralinos if they had not decayed further into LSPs. Since the gravitino is weakly interacting, we assume that all the heavier SUSY particles decay into the LSP via the NLSP. This process increases the abundance of gravitinos and is referred to as non-thermal production of gravitinos when the system is out of equilibrium. Therefore, the current dark matter relic density will be related to both the LSP and NLSP densities. As stated earlier, the NLSP relic density can be found using Boltzmann statistics. In chemical equilibrium, we have an equilibrium number density of neutralinos, n_χ^{eq}, given by (2.7) with $A \to \chi$. When out of equilibrium, the number density will change according to the Boltzmann equation [14]

$$\frac{dn_\chi}{dt} = -3Hn_\chi - \langle \sigma^{ann} v \rangle \left(n_\chi^2 - (n_\chi^{eq})^2 \right) \tag{3.26}$$

where the angle brackets describe the thermal average of the annihilation cross section times the velocity. This factor tends to zero as the cross section tends to zero, and thus describes freeze out for neutralinos. Introducing the variables to account for entropy conservation

$$Y_\chi \equiv \frac{n_\chi}{s}, \quad Y_\chi^{eq} \equiv \frac{n_\chi^{eq}}{s}, \quad x \equiv \frac{m_\chi}{T} \tag{3.27}$$

the above expression can be rewritten as

$$\frac{dY_\chi}{dx} = -\frac{\langle \sigma^{ann} v \rangle s}{Hx} (Y_\chi^2 - (Y_\chi^{eq})^2) \tag{3.28}$$

Now, we can calculate the neutralino relic density using the relation [15]

$$\Omega_\chi h^2 = \frac{m_\chi s_0 Y_{\chi,0} h^2}{\rho_{C,0}} = 2.755 \times 10^8 \left(\frac{m_\chi Y_{\chi,0}}{1 \text{ GeV}} \right) \tag{3.29}$$

where zero denotes the current value. Thus, the total dark matter density is given as the sum of the thermal and non-thermal production of gravitinos

$$\Omega_{DM} h^2 = \Omega_{3/2} h^2 + \frac{m_{3/2}}{m_\chi} \Omega_\chi h^2 \tag{3.30}$$

Chapter 4

Neutralino Branching Ratio

As we consider the gravitino the lightest supersymmetric particle, we want to know how the lightest neutralino can decay into a gravitino and produce the dark matter abundance that we currently observe. This is especially important, as the BBN constraints are dependent not only on the mass of the decaying particle, but also the interactions and decay channels.

In the following subsections, the decay channels we have stated can be calculated from the Feynman rules given in [11]. The result of these calculations can also be found in [11], but not the calculations themselves. As a consequence, we have added an example on such a calculation in Appendix B.

4.1   Primary Gaugino Contribution

The gaugino $(\widetilde{G})$, the linear combination of $\widetilde{B}$ and $\widetilde{W}^0$ with mass $m_{\widetilde{G}}$, can decay into a gravitino and a photon, with the following channel

$$\Gamma(\widetilde{G} \rightarrow \Psi_{3/2}\gamma) = \frac{|N_{11}c_W + N_{12}s_W|^2}{48\pi M_p^2} \frac{m_{\widetilde{G}}^5}{m_{3/2}^2}(1 - x_{3/2}^2)^3(1 + 3x_{3/2}^2) \qquad (4.1)$$

where $x_{3/2} = m_{3/2}/m_{\widetilde{G}}$. This channel is always allowed as the photon is massless. The gaugino can also decay into a gravitino and a Z boson, via

$$
\begin{aligned}
\Gamma(\widetilde{G} \to \Psi_{3/2}Z) =& \frac{|-N_{11}s_W + N_{12}c_W|^2}{48\pi M_p^2} \frac{m_{\widetilde{G}}^5}{m_{3/2}^2} \\
&\times [1 - 2(x_{3/2}^2 + x_Z^2) + (x_{3/2}^2 - x_Z^2)^2]^{\frac{1}{2}} \\
&\times [(1 - x_{3/2}^2)^2(1 + 3x_{3/2}^2) - x_Z^2\{3 + x_{3/2}^3(x_{3/2} - 12) \\
&- x_Z^2(3 - x_{3/2}^2 - x_Z^2)\}]
\end{aligned}
\tag{4.2}
$$

where $x_Z = m_Z/m_{\widetilde{G}}$. This channel is only allowed if $m_{\widetilde{G}} > m_{3/2} + m_Z$.

The electromagnetic branching ratio for gaugino decays is easy to find, as the only major contribution to non-EM decays is the $Z \to \nu\bar{\nu}$ channel, and therefore, a good approximation is $B_{EM}^{\widetilde{G}} \simeq 1$. The hadronic branching ratio is dependent on the Z channel and the off-shell photon channel, and is given by

$$
B_{had}^{\widetilde{G}} \simeq \frac{\Gamma(\widetilde{G} \to \Psi_{3/2}Z)B_{had}^Z + \sum_q \Gamma(\widetilde{G} \to \Psi_{3/2}\gamma^* \to q\bar{q})}{\Gamma(\widetilde{G} \to \Psi_{3/2}Z) + \Gamma(\widetilde{G} \to \Psi_{3/2}\gamma)}
\tag{4.3}
$$

where the off-shell photon decay channel is given by

$$
\Gamma(\widetilde{G} \to \Psi_{3/2}\gamma^* \to q\bar{q}) \simeq \alpha_{EM} \frac{|N_{11}c_W + N_{12}s_W|^2 Q^2}{6(2\pi)^2 M_p^2} \frac{m_{\widetilde{G}}^5}{m_{3/2}^2} \ln\left(\frac{m_{\widetilde{G}}}{2m_q}\right)
\tag{4.4}
$$

with Q defined as the quark's electric charge, m_q is the quark mass, and α_{EM} as the EM coupling constant. Here we can see that the off-shell photon channel is enhanced by a logarithmic IR-divergence, thus keeping the hadronic branching ratio present even at low masses. This channel is dominated by the up quark, as it is the lightest quark in addition to its charge of $Q = 2/3$. The gaugino can also decay into quarks via an off-shell Z boson, W^+W^-, or a squark, but these channels can safely be ignored as their contributions are small.

From the primary decay channels, we can give an approximate expression for the lifetime of a massive gaugino assuming an equal bino and wino contribution i.e. $N_{11} = N_{12} = 1/\sqrt{2}$

$$
\Gamma^{-1}(\widetilde{G} \to \Psi_{3/2}\gamma/Z) \simeq 59 \text{ s} \left(\frac{1 \text{ TeV}}{m_{\widetilde{G}}}\right)^5 \left(\frac{m_{3/2}}{10 \text{ GeV}}\right)^2
\tag{4.5}
$$

24

4.2 Primary Higgsino Contribution

The Higgsino ($\widetilde{H}$), the linear combination of $\widetilde{H}_d^0$ and $\widetilde{H}_u^0$ with mass $m_{\tilde{H}}$, cannot decay into a photon at tree level, but can decay into a gravitino and a Z boson, with the following decay rate

$$
\begin{aligned}
\Gamma(\widetilde{H} \to \Psi_{3/2}Z) = & \frac{|-N_{13}c_\beta + N_{14}s_\beta|^2}{96\pi M_p^2} \frac{m_{\widetilde{H}}^5}{m_{3/2}^2}[1 - 2(x_{3/2}^2 + x_Z^2) + (x_{3/2}^2 - x_Z^2)^2]^{\frac{1}{2}} \\
& [(1 + x_{3/2})^2(1 - x_{3/2})^4 - x_Z^2\{(1 - x_{3/2})^2(3 + 2x_{3/2} - 9x_{3/2}^2) \\
& -x_Z^2(3 - 2x_{3/2} - 9x_{3/2}^2 - x_Z^2)\}]
\end{aligned}
$$

(4.6)

where x_i is the mass ratio of the mass of particle i with respect to $m_{\widetilde{H}}$. This channel is only allowed if $m_{\widetilde{H}} > m_{3/2} + m_Z$. Since there is no interference between the Z channels of the Higgsino and the gaugino, the total Z channel of the neutralino is simply the sum of both channels, with $m_{\widetilde{G}}, m_{\widetilde{H}} \to m_\chi$. The Higgsino can also decay into the light, heavy, and pseudo-scalar Higgs respectively via

$$
\begin{aligned}
\Gamma(\widetilde{H} \to \Psi_{3/2}h) = & \frac{|-N_{13}s_\alpha + N_{14}c_\alpha|^2}{96\pi M_p^2} \frac{m_{\widetilde{H}}^5}{m_{3/2}^2}[1 - 2(x_{3/2}^2 + x_h^2) + (x_{3/2}^2 - x_h^2)^2]^{\frac{1}{2}} \\
& [(1 - x_{3/2})^2(1 + x_{3/2})^4 - x_h^2\{(1 + x_{3/2})^2(3 - 2x_{3/2} + 3x_{3/2}^2) \\
& -x_h^2(3 + 2x_{3/2} + 3x_{3/2}^2 - x_h^2)\}]
\end{aligned}
$$

(4.7)

$$
\begin{aligned}
\Gamma(\widetilde{H} \to \Psi_{3/2}H) = & \frac{|N_{13}c_\alpha + N_{14}s_\alpha|^2}{96\pi M_p^2} \frac{m_{\widetilde{H}}^5}{m_{3/2}^2}[1 - 2(x_{3/2}^2 + x_H^2) + (x_{3/2}^2 - x_H^2)^2]^{\frac{1}{2}} \\
& [(1 - x_{3/2})^2(1 + x_{3/2})^4 - x_H^2\{(1 + x_{3/2})^2(3 - 2x_{3/2} + 3x_{3/2}^2) \\
& -x_H^2(3 + 2x_{3/2} + 3x_{3/2}^2 - x_H^2)\}]
\end{aligned}
$$

(4.8)

$$\Gamma(\widetilde{H} \to \Psi_{3/2}A) = \frac{|N_{13}s_\beta + N_{14}c_\beta|^2}{96\pi M_p^2} \frac{m_{\widetilde{H}}^5}{m_{3/2}^2} [1 - 2(x_{3/2}^2 + x_A^2) + (x_{3/2}^2 - x_A^2)^2]^{\frac{1}{2}}$$

$$[(1 + x_{3/2})^2(1 - x_{3/2})^4 - x_A^2\{(1 - x_{3/2})^2(3 + 2x_{3/2} + 3x_{3/2}^2)$$

$$-x_A^2(3 - 2x_{3/2} + 3x_{3/2}^2 - x_A^2)\}]$$

$$(4.9)$$

where $x_i = m_i/m_{\widetilde{H}}$.

Again, as the only contribution to non-EM decays is via $Z \to \nu\bar{\nu}$, the electromagnetic branching ratio is simply $B_{EM}^{\widetilde{H}} \simeq 1$, and the hadronic branching ratio is given by

$$B_{had}^{\widetilde{H}} \simeq \frac{\Gamma(\widetilde{H} \to \Psi_{\frac{3}{2}}Z)B_{had}^Z + \Gamma(\widetilde{H} \to \Psi_{\frac{3}{2}}h)B_{had}^h}{\Gamma(\widetilde{H} \to \Psi_{\frac{3}{2}}Z) + \Gamma(\widetilde{H} \to \Psi_{\frac{3}{2}}h) + \Gamma(\widetilde{H} \to \Psi_{\frac{3}{2}}H) + \Gamma(\widetilde{H} \to \Psi_{\frac{3}{2}}A)}$$
$$(4.10)$$

There are also some Higgsino 4-vertex decay channels available, which we will ignore in this thesis, as their contributions are small.

Using the primary decay channels, and since the decays to the heavy Higgses are subdominant, we can approximate the lifetime of a heavy Higgsino in the decoupling limit, $\sin\alpha = -\cos\beta$, $\cos\alpha = \sin\beta$, using $\tan\beta = 10$ and $N_{13} = N_{14} = 1/\sqrt{2}$ as such

$$\Gamma^{-1}(\widetilde{H} \to \Psi_{3/2}Z/h) \simeq 118 \text{ s} \left(\frac{\text{TeV}}{m_{\widetilde{H}}}\right)^5 \left(\frac{m_{3/2}}{10 \text{ GeV}}\right)^2 \qquad (4.11)$$

Chapter 5

BBN Constraints

As the gravitino is the LSP, the effects of it decaying during or after BBN
will not occur, which makes the gravitino a good candidate for dark matter.
Instead, we will focus on the neutralino relic density as it will be constrained
by BBN, as explained previously. This will limit the available parameter
space for a general gravitino LSP, neutralino NLSP model. In [16], this was
done with input parameters defined in the low energy regime. In this thesis,
we will expand on that result by defining the input parameters in the high
energy regime, to see if the scale at which the parameters are defined, is
important for the results. We will also introduce a non-unity dilution factor
to see if that is a possible approach to the gravitino problem mentioned in
Section 3.2.

To calculate the relic density of the NLSP, $\Omega_\chi h^2$, we will use the numerical
package micrOMEGAs 4.3.1 [17] which uses (3.26) to calculate Ω_χ, with
SuSpect 2.41 [18] to calculate the physical mass spectrum, that is, using the
renormalization group equations (3.15) and (3.17) to find the masses in the
relevant energy regime. We will fix the mass parameters at 2.2 TeV, set the
scalar couplings to 0, $\tan\beta$ to 10, and vary M_1 and M_2. We will also vary μ,
but due to software restrictions, only as a low energy input parameter.

When we vary the parameters, it is useful to notice that M_2 and μ are
restricted from below at 100 GeV from Large Electron Positron Collider

(LEP) searches. This comes from the fact that the wino and Higgsino can decay into charged W and charged Higgs bosons respectively, which are easier to find in a lepton collider. Therefore M_1 is not bound by LEP searches, as the bino does not have a tree level vertex involving charged particles. These bounds are not affected by the LHC as hadrons do not generally do very well to probe specific energies. Therefore, even if nothing were found at a given LHC energy level, we cannot conclude that nothing is there.

Lastly, the constraints we are using are the same as in the low energy plots. These are extracted as individual points from the figures FIG. 9 and FIG. 10 in [7], and plotted in our plots with lines drawn between the points. The EM bound is extracted using $B_{had} = 0$, and the hadronic bounds are extracted using $B_{had} = 1$ and its less conservative bound for the different masses.

5.1   Bino-Wino NLSP

First, we consider the scenario where the NLSP is mainly a superposition of a bino and a wino interaction state. Therefore, we fix $\mu = 3$ TeV, and vary M_1 and M_2 between 0.1 and 3 TeV. Note that there is still a small Higgsino component present in the NLSP as we consider a finite μ. Figure 5.1 shows the result when we input the parameters at the low energy scale. Inputting the parameters at the high energy scale, we obtain Figure 5.2. Both of these figures use $\Delta = 1$ in accordance with standard cosmology. An interesting observation is that at the low energy scale, we find that $M_1 \simeq M_2$ leads to an equal composition of bino and wino in the NLSP, but at the high energy scale, the relation changes to $M_2 \simeq 0.54 M_1$. This change can be explained by the difference between b_1 and b_2 in (3.15).

When we compare the two aforementioned figures with each other, the first thing we notice is that similarly to the low energy plots, the high energy plots have a large dip in the high mass area. We also notice two extra dips in the low mass area. If we look closely on the low energy plots, we

can in fact see something that resemble these to low mass dips too, even though it's only a few points. The leftmost dip corresponds to, as in the low energy regime, annihilations into the pseudo-scalar Higgs for neutralinos with $m_\chi \simeq 1.1$ TeV, which is an open channel due to the presence of a small Higgsino component in the NLSP. The middle and rightmost dips correspond to resonant annihilations into the light scalar Higgs and the Z boson as the neutralinos have mass $m_\chi \simeq 61$ GeV and $m_\chi \simeq 44$ GeV respectively, which is about half the mass of these particles. The fact that we observe these resonances in the high energy regime can be explained by looking at (3.15). This equation tells us that if we use the same parameters in the high energy regime compared to the low energy regime, we end up with a lighter NLSP in the reference scale for the high energy regime. This behaviour is the reason why we have to go up to 3 TeV parameters to find the pseudo-scalar Higgs resonance. There is also a new feature in the high energy plots that we do not see in the low energy plots, and that is an asymptotic tendency in the light wino-dominated regime, in which the given parameters actually results in perturbation problems and/or Landau poles.

Secondly, similarly to the low energy plots, the hadronic bounds are generally more constraining, where only very light wino-dominated states and very heavy states with a significant wino contribution are allowed. These are the areas of the asymptotic divergence, and below the pseudo-scalar Higgs resonance. Analysing the plots for $m_{3/2} = 10$ GeV, we see that even though a light wino is not hadronically bounded, the EM bound will constrain it, however, there is a slight possibility that the asymptotic tendency will continue into the non-constrained area and make a light wino a possible NLSP. The heavy wino-like state is however, still unconstrained regarding both hadronic and EM constraints. In the case when $m_{3/2} = 1$ GeV, the constraints are a bit more relaxed. A light wino-like NLSP is more or less allowed, and the allowed parameter space for a heavy wino-like NLSP has greatly increased to include more of the bino-dominated NLSP.

In Figure 5.3, we have plotted the high energy case using the conservative

bound from leptogenesis $\Delta = 8 \times 10^3$ in comparison [19]. As we can see in the plots for both $m_{3/2} = 1$ GeV and $m_{3/2} = 10$ GeV cases, the allowed parameter space has severely increased. The entire lower part of the plots as well as all the heavy neutralinos have become allowed states. For a $m_{3/2} = 1$ GeV gravitino, the light Higgs resonance is not entirely illegal as it is below the conservative hadronic bounds, which certainly is not the case for a $m_{3/2} = 10$ GeV gravitino, as this area is ruled out by the EM bound.

An interesting observation from these plots is that if we increase the mass of the gravitino, we see that the only difference would be that all the points move towards higher lifetime equally far on the log scale. The implications from this fact is that for a $\Delta = 1$ massive gravitino model, every point would be excluded, but for $\Delta = 8 \times 10^3$, the entire lower half of the plots would still be allowed. This means that models with gravitino mass $m_{3/2} \geq 100$ GeV is still allowed as long as the neutralino has a large wino component.
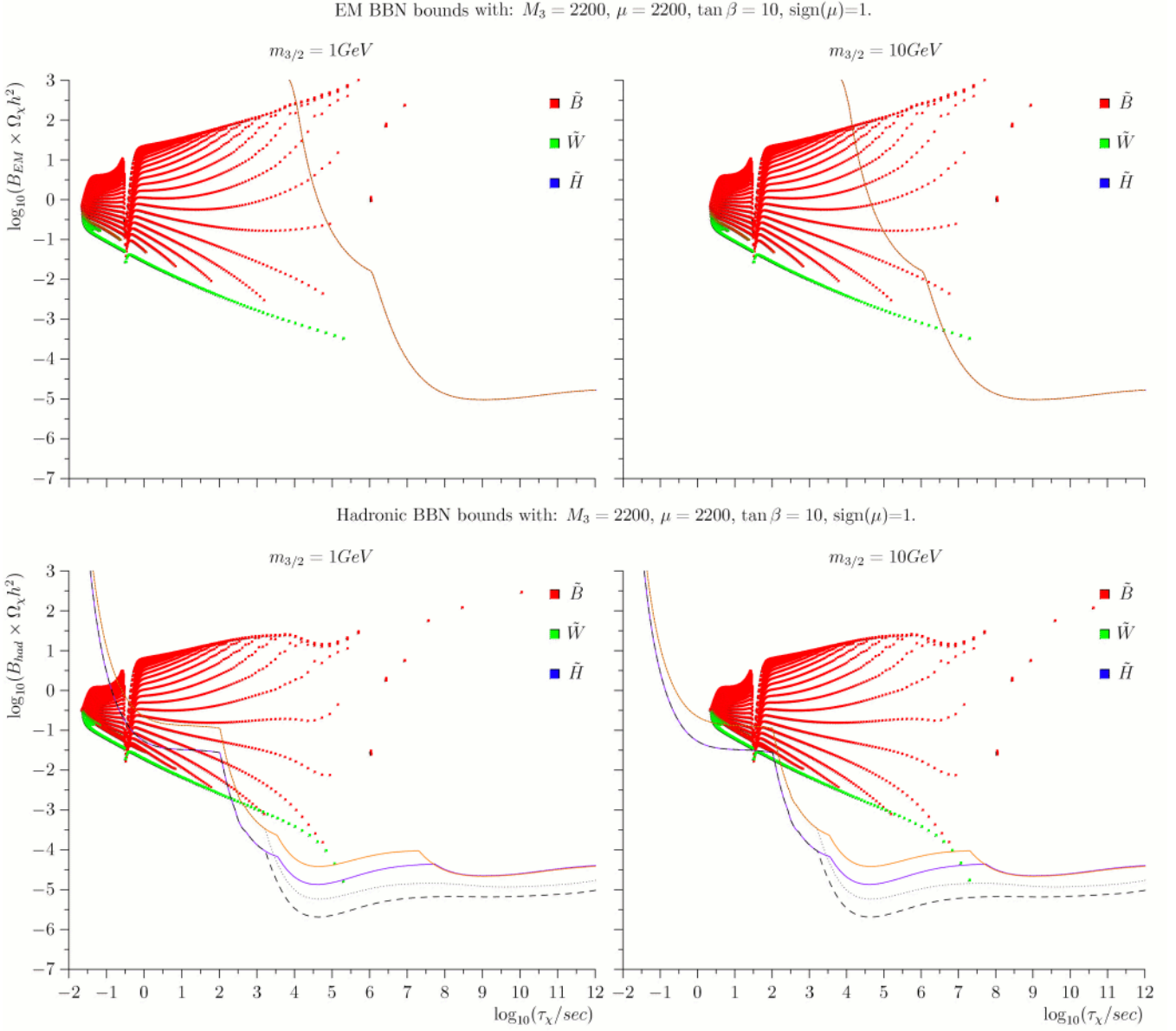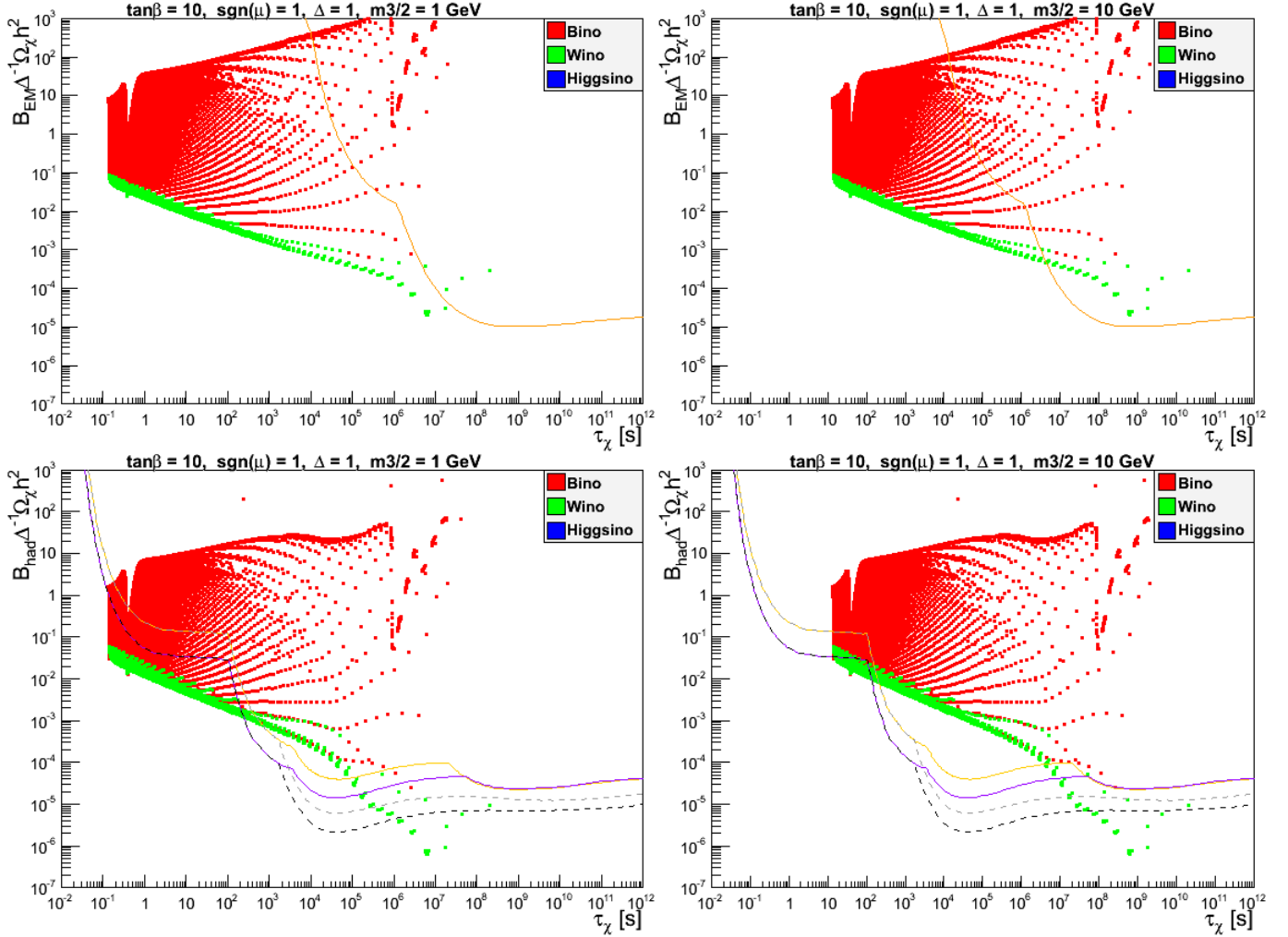
Figure 5.1: Relic density of bino-wino NLSP compared to the BBN electromagnetic (top) and hadronic (bottom) constraints in the case of a 1 (left) and 10 (right) GeV gravitino LSP mass in the low energy scale. The continuous (dashed) lines corresponds to more (less) conservative bounds for the ^{6}Li to ^{7}Li ratio. The orange/upper and purple/lower lines correspond to constraints on a 1 TeV and 100 GeV decaying particle mass. The mass increases from right to left, and the composition goes from bino at the top to wino at the bottom. The graphs are taken from [16].
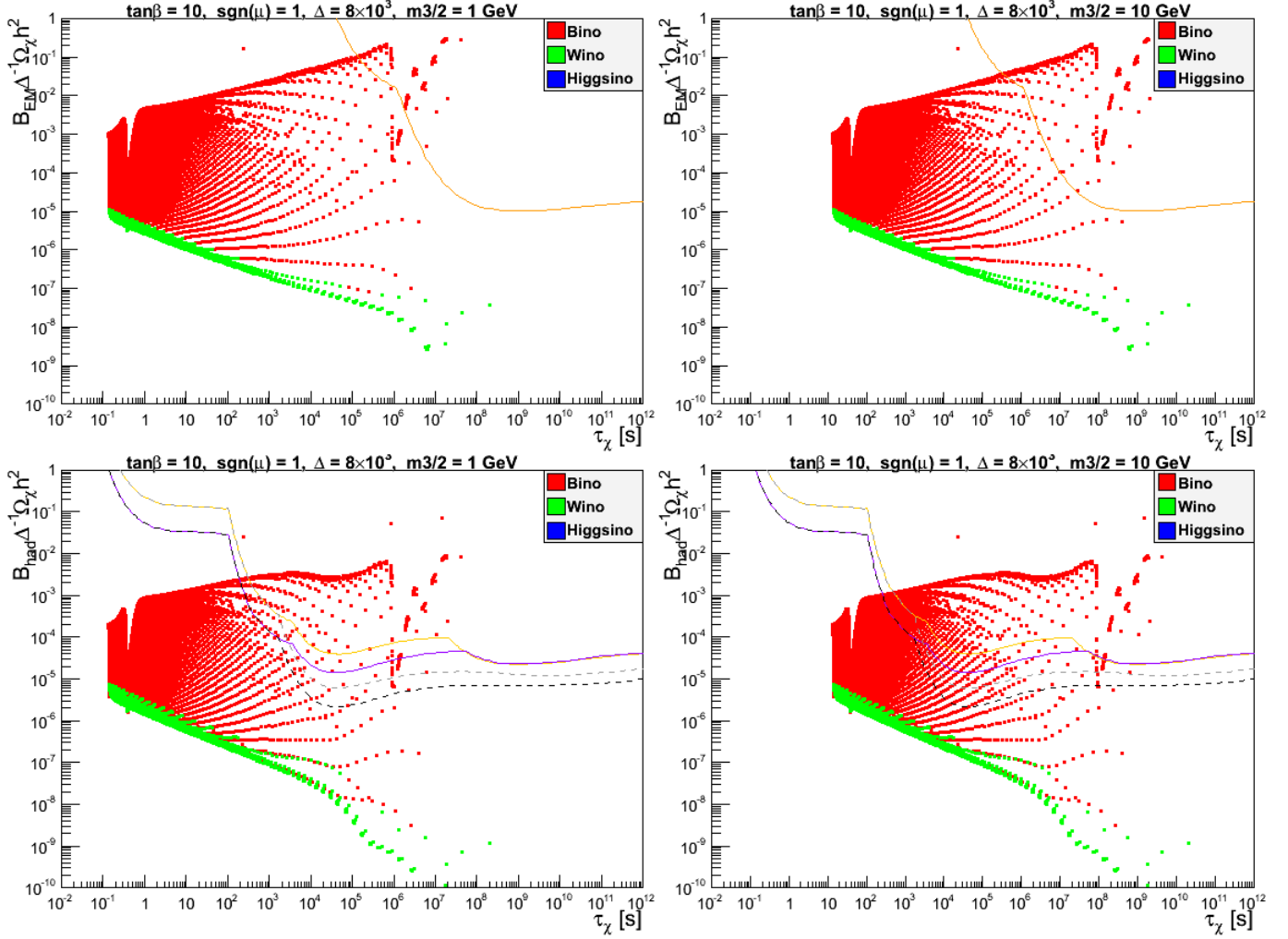
31

Figure 5.2: Relic density of bino-wino NLSP compared to the BBN electromagnetic (top) and hadronic (bottom) constraints in the case of a 1 (left) and 10 (right) GeV gravitino LSP mass in the high energy scale. The continuous (dashed) lines corresponds to more (less) conservative bounds for the ^{6}Li to ^{7}Li ratio. The orange/upper and purple/lower lines correspond to constraints on a 1 TeV and 100 GeV decaying particle mass. The mass increases from right to left, and the composition goes from bino at the top to wino at the bottom.

32

Figure 5.3: Relic density for of bino-wino NLSP compared to the BBN electromagnetic (top) and hadronic (bottom) constraints in the case of a 1 (left) and 10 (right) GeV gravitino LSP mass in the high energy scale for a non-unity Δ. The continuous (dashed) lines corresponds to more (less) conservative bounds for the ^{6}Li to ^{7}Li ratio. The orange/upper and purple/lower lines correspond to constraints on a 1 TeV and 100 GeV decaying particle mass. The mass increases from right to left, and the composition goes from bino at the top to wino at the bottom.

33

5.2 Bino-Higgsino NLSP

Now we consider the scenario where the NLSP is mainly a combination of a bino and a Higgsino interaction state. Therefore, we fix $M_2 = 3$ TeV and vary M_1 and μ between 0.1 and 3 TeV. Figure 5.4 shows the result when we input the parameters at the low energy scale. Inputting the parameters at the high energy scale, we obtain Figure 5.5. Both of these figures use $\Delta = 1$ in accordance with standard cosmology. In this scenario, we find that at the low energy scale, $\mu \simeq M_1$ still leads to an equal composition of bino and Higgisno in the NLSP, but at the high energy scale, the relation changes to $\mu \simeq 0.43M_1$. This can be explained by the fact that M_1 will be shifted down by (3.15), but μ will stay constant, as it is input as a low energy parameter. Therefore, we have to manually shift μ down to account for the change in M_1.

In the figures referenced above, we see the similarities in the high versus low energy bino-Higgsino NLSP plots, and also the similarities in the high energy bino-wino and bino-Higgsino NSLP plots. In both Figure 5.2 and Figure 5.5, we find the pseudo-scalar Higgs resonance, but in the bino-Higgsino case, it is much more noticeable, as it stretches far below the lower Higgsino band. This is a result of the high Higgsino contribution to the NLSP, combined with the fact that we also get a noticeable heavy scalar Higgs annihilation resonance in the same area, as the two resonances are degenerate. This is the same behaviour as in the low energy case.

In the lower end of the mass spectrum in the high energy plots, we find the same behaviour as in the low energy plots, and also, we find the imprints of the low mass resonances in this area, the same resonances seen in Figure 5.2. These resonances can also be seen in the low energy bino-Higgsino plots, but cannot be distinguished from each other, as the resolution is too low. In the low mass scale we also observe a significant difference between Figure 5.5 and Figure 5.2, which is that the asymptotic divergence observed in the bino-wino plots is missing in the bino-Higgsino plots, as μ does not need to

be renormalized, since it is a low energy input parameter.

Similarly to the bino-wino plots, the high energy bino-Higgsino is more constrained by the hadronic bounds, as only part of the resonances are not bound hadronically, together with the most massive Higgsino-like NLSPs. For a gravitino mass $m_{3/2} = 10$ GeV, we can see that even though a medium to heavy NLSP is allowed regarding the EM bounds, and a light bino with a large Higgsino component is barely allowed regarding the conservative hadronic bounds, the only part that satisfies both constraints is the area of the pseudo-scalar Higgs resonance. In the $m_{3/2} = 1$ GeV case, things look a bit brighter. A light bino with a large Higgsino component, corresponding to the lower part of the light Higgs resonance, is barely allowed regarding both the EM bound and conservative hadronic bounds, and a heavy NLSP in the pseudo-scalar Higgs resonance area is allowed as the points are right below the hadronic bound. More bino-like compositions of a heavy NLSP is allowed by the EM BBN bound, but ruled out by the hadronic bounds.

In Figure 5.6, we have plotted the high energy regime again, with $\Delta = 8 \times 10^3$ instead. Now we see that a $m_{3/2} = 10$ GeV is much more plausible, as a heavy NLSP is allowed with respect to both bounds, and the entire bottom part of the plot is pushed below the constraints, and thus contain allowed states. In the $m_{3/2} = 1$ GeV case, the allowed parameter space is almost unscathed regarding the EM constraint, and only the light most bino-like NLSPs are disallowed by the conservative hadronic bounds, and therefore, almost the entire parameter space for a $m_{3/2} = 1$ GeV gravitino is allowed.

Similarly to high energy bino-wino plots, we can extrapolate the results of a larger gravitino mass. In the case $\Delta = 1$, we see that if we increase the gravitino mass, the entire plot moves out of the unconstrained area, and therefore, there are no allowed points. For a $\Delta = 8 \times 10^3$, the outlook is much more interesting. We see that even if me move the plot toward higher lifetimes, the entire lower part of the plot would still be unconstrained, and therefore still allow Higgsino-like NLSPs for $m_{3/2} \geq 100$ GeV.
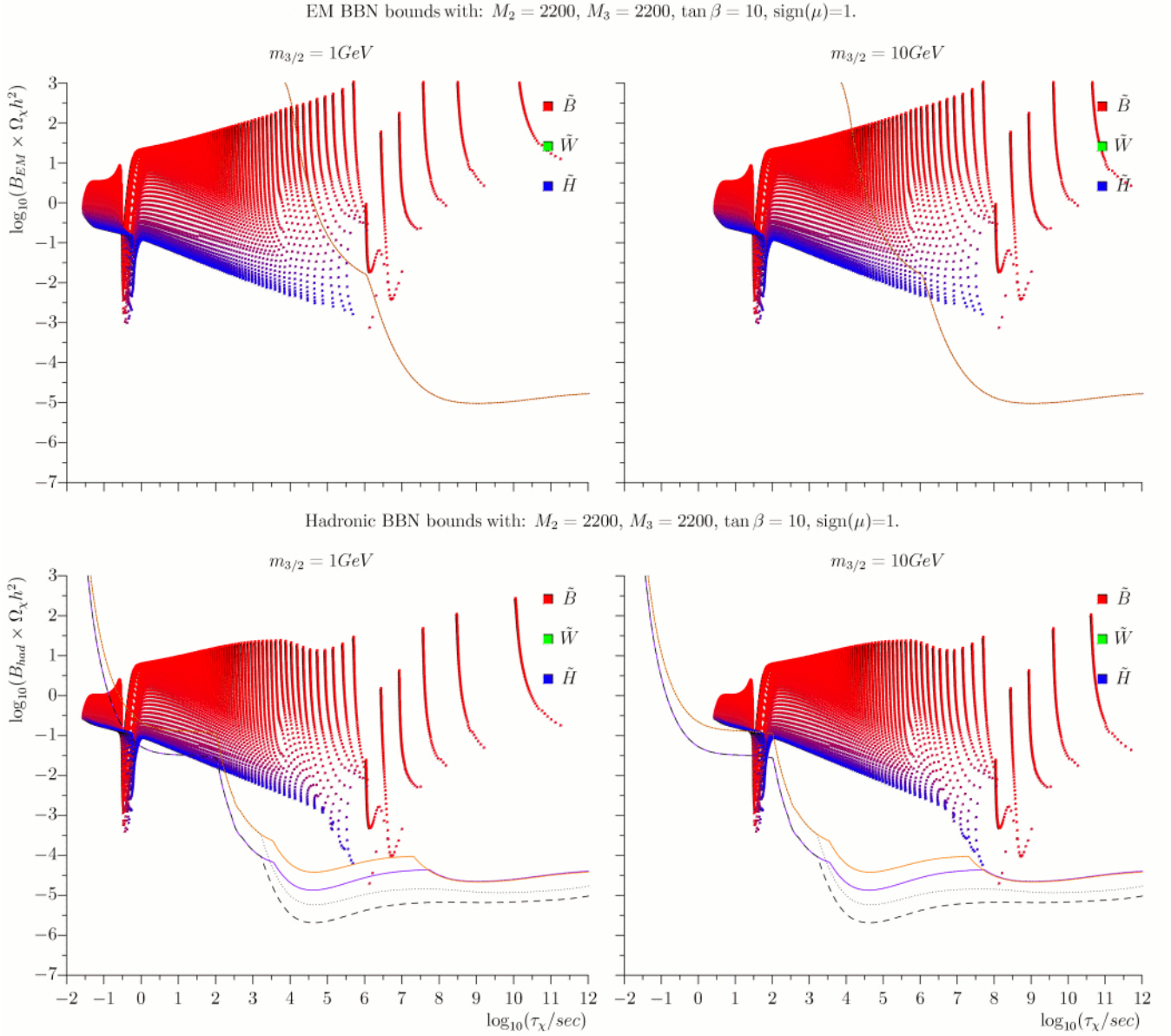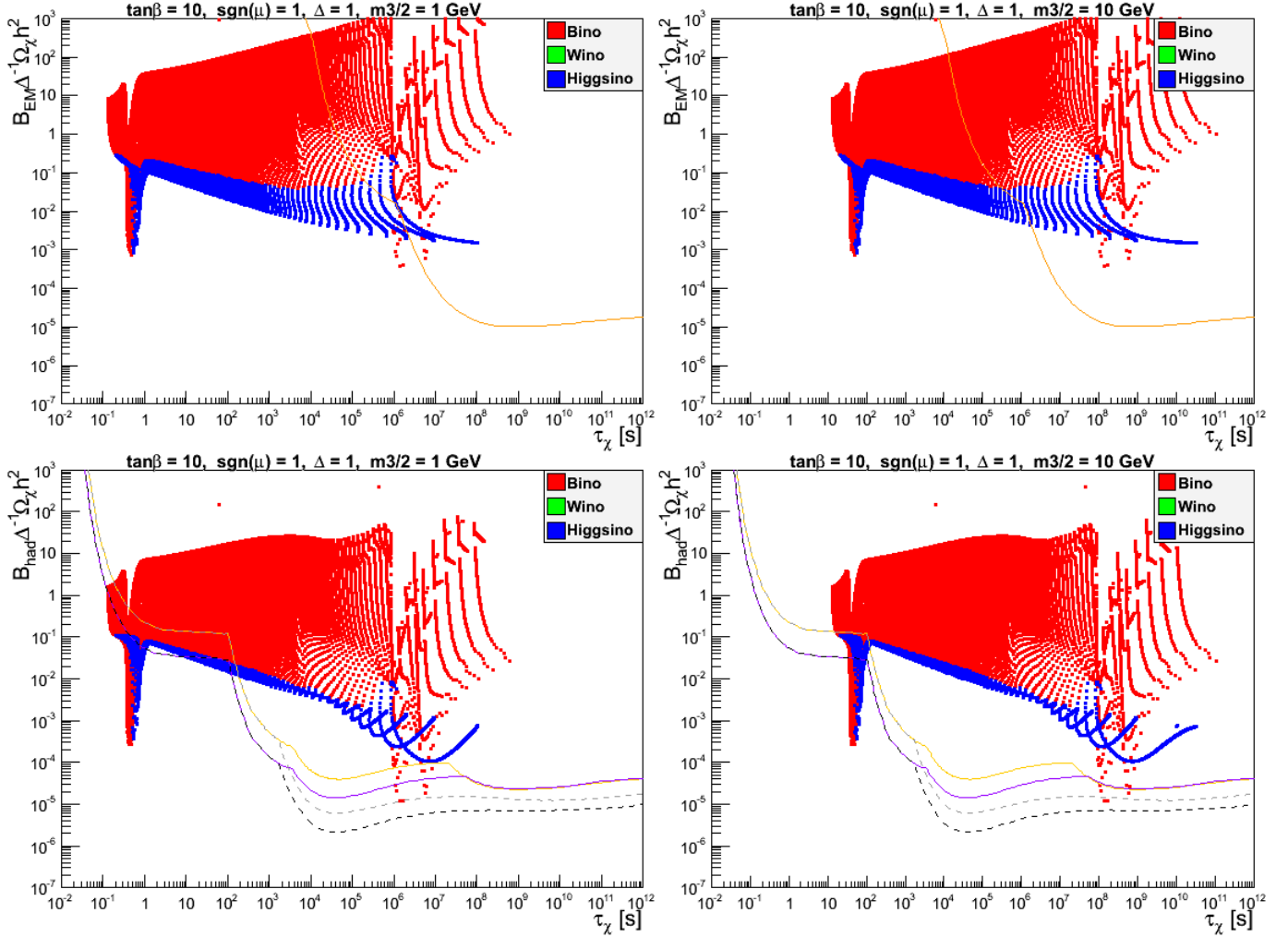
Figure 5.4: Relic density of bino-Higgsino NLSP compared to the BBN electromagnetic (top) and hadronic (bottom) constraints in the case of a 1 (left) and 10 (right) GeV gravitino LSP mass in the low energy scale. The continuous (dashed) lines corresponds to more (less) conservative bounds for the ^{6}Li to ^{7}Li ratio. The orange/upper and purple/lower lines correspond to constraints on a 1 TeV and 100 GeV decaying particle mass. The mass increases from right to left, and the composition goes from bino at the top to Higgsino at the bottom. The graphs are taken from [16].
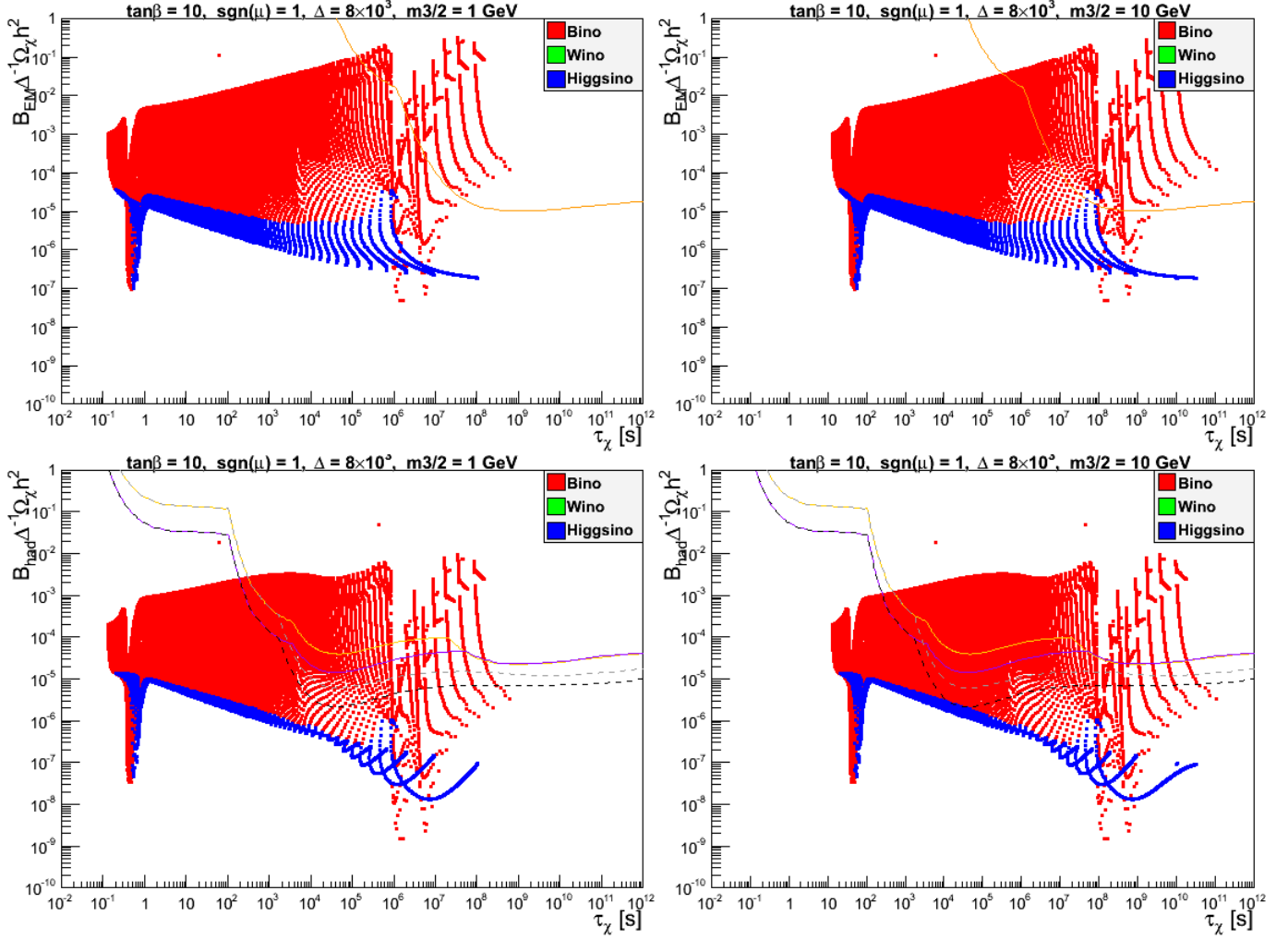
Figure 5.5: Relic density of bino-Higgsino NLSP compared to the BBN electromagnetic (top) and hadronic (bottom) constraints in the case of a 1 (left) and 10 (right) GeV gravitino LSP mass in the high energy scale. The continuous (dashed) lines corresponds to more (less) conservative bounds for the ^{6}Li to ^{7}Li ratio. The orange/upper and purple/lower lines correspond to constraints on a 1 TeV and 100 GeV decaying particle mass. The mass increases from right to left, and the composition goes from bino at the top to Higgsino at the bottom.

Figure 5.6: Relic density of bino-Higgsino NLSP compared to the BBN electromagnetic (top) and hadronic (bottom) constraints in the case of a 1 (left) and 10 (right) GeV gravitino LSP mass in the high energy scale for a non-unity Δ. The continuous (dashed) lines corresponds to more (less) conservative bounds for the ^{6}Li to ^{7}Li ratio. The orange/upper and purple/lower lines correspond to constraints on a 1 TeV and 100 GeV decaying particle mass. The mass increases from right to left, and the composition goes from bino at the top to Higgsino at the bottom.

5.3   Wino-Higgsino NLSP

Now we consider the scenario where the NLSP is mainly a combination of a wino and a Higgsino interaction state. Therefore, we fix $M_2 = 3$ TeV and vary M_1 and μ between 0.1 and 3 TeV. Figure 5.7 shows the result when we input the parameters at the low energy scale. Inputting the parameters at the high energy scale, we obtain Figure 5.8. Both of these figures use $\Delta = 1$ in accordance with standard cosmology. Again, in the low energy regime, $\mu \simeq M_2$ leads to an equal composition of wino and Higgsino, but in the high energy regime, the relation is $\mu \simeq 0.80 M_2$. This is as expected, as M_1 shifts more from high energy to low energy scale than M_2, and μ does not shift at all, which we have explained in the previous two scenarios.

If we compare the high energy plots to the low energy plots, we find many similarities in the plots. The only differences are that in the high energy limit, the plots reach further towards the low NLSP mass range to reveal the same asymptotic behaviour found in Figure 5.2, and a small area towards the highest NLSP mass with mainly a bino component, which is a result of the limits used for the primary parameters. This is to be expected, as input parameters close to each other, $M_1 \simeq M_2 \simeq \mu$, will result in a NLSP with a high bino composition. Other than those differences, we recognize the same pseudo-scalar Higgs resonance, and generally similar structure of points within the plots.

Again, in the high energy wino-Higgsino NLSP plots, the hadronic bounds are more constraining. We observe that for a gravitino mass $m_{3/2} = 10$ GeV, a light wino NLSP in the asymptotic area will be unaffected by neither the hadronic nor the EM constraints, and is therefore an allowed state. The same holds for a heavy NLSP in the pseudo-scalar Higgs resonance area, and is also allowed. In the case of $m_{3/2} = 1$ GeV, we see that almost the entire wino band has become allowed except for a small range in the medium NLSP mass regime. Also a large amount of the heavy Higgsino-dominated NLSPs have been pushed to the left of the constraints into the allowed area, together

with the heavy bino-dominated NLSPs.

We have also plotted the high energy case with $\Delta = 8 \times 10^3$, as for the other cases, in Figure 5.9. Here, we can see that the entire plot has moved below the constraints and every point is therefore allowed. We also notice, as with the other cases, that if we increase the gravitino mass, the entire plot will just move towards longer lifetimes. For $\Delta = 1$, the light winos near the asymptotic divergence will stay below the bounds and therefore remain allowed. In the $\Delta = 8 \times 10^3$ case, the entire plot will remain below the constraint, with the exception of the bino NLSPs.
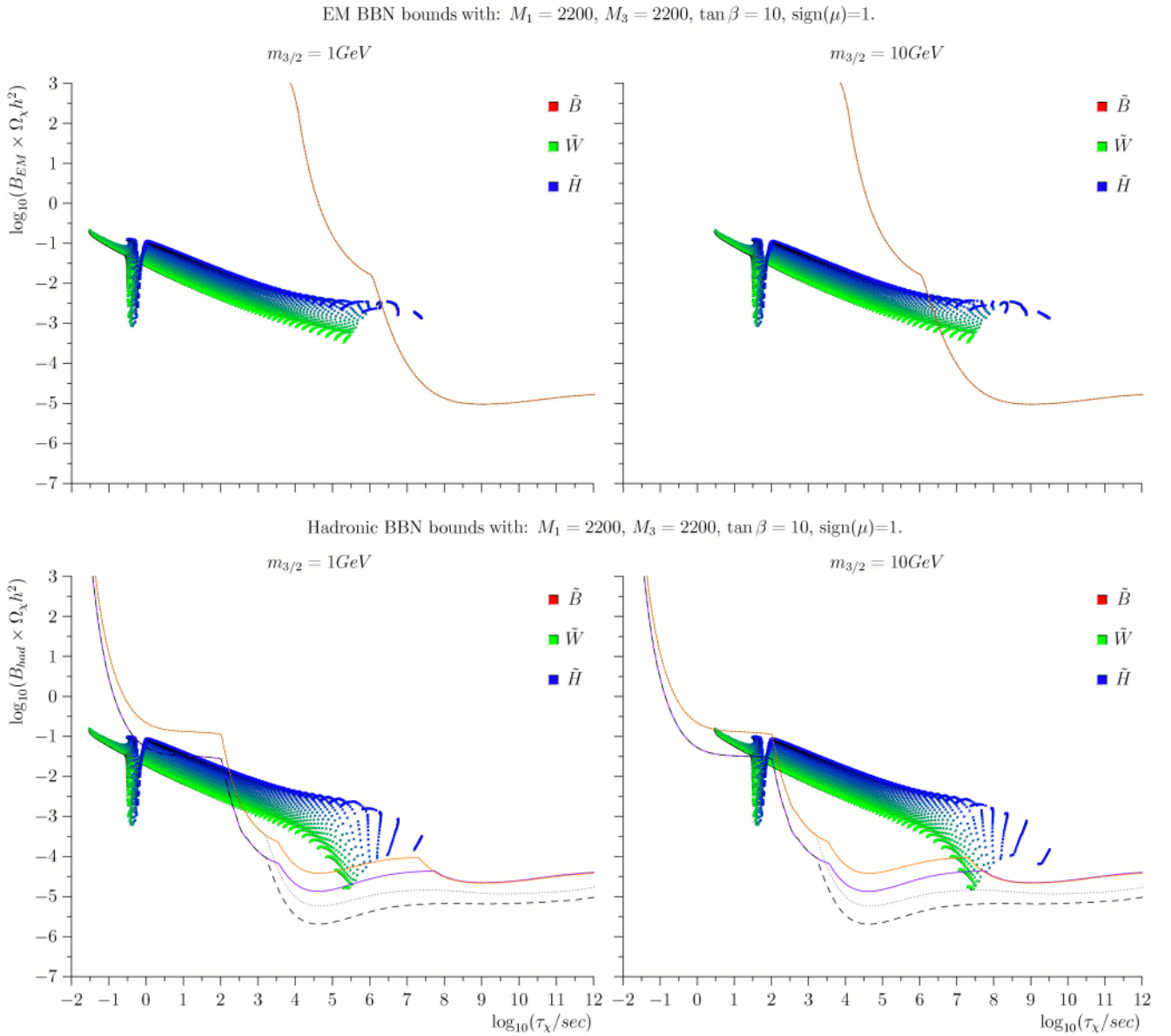
Figure 5.7: Relic density of wino-Higgsino NLSP compared to the BBN electromagnetic (top) and hadronic (bottom) constraints in the case of a 1 (left) and 10 (right) GeV gravitino LSP mass in the low energy scale. The continuous (dashed) lines corresponds to more (less) conservative bounds for the ^{6}Li to ^{7}Li ratio. The orange/upper and purple/lower lines correspond to constraints on a 1 TeV and 100 GeV decaying particle mass. The mass increases from right to left, and the composition goes from Higgsino at the top to wino at the bottom. The graphs are taken from [16].
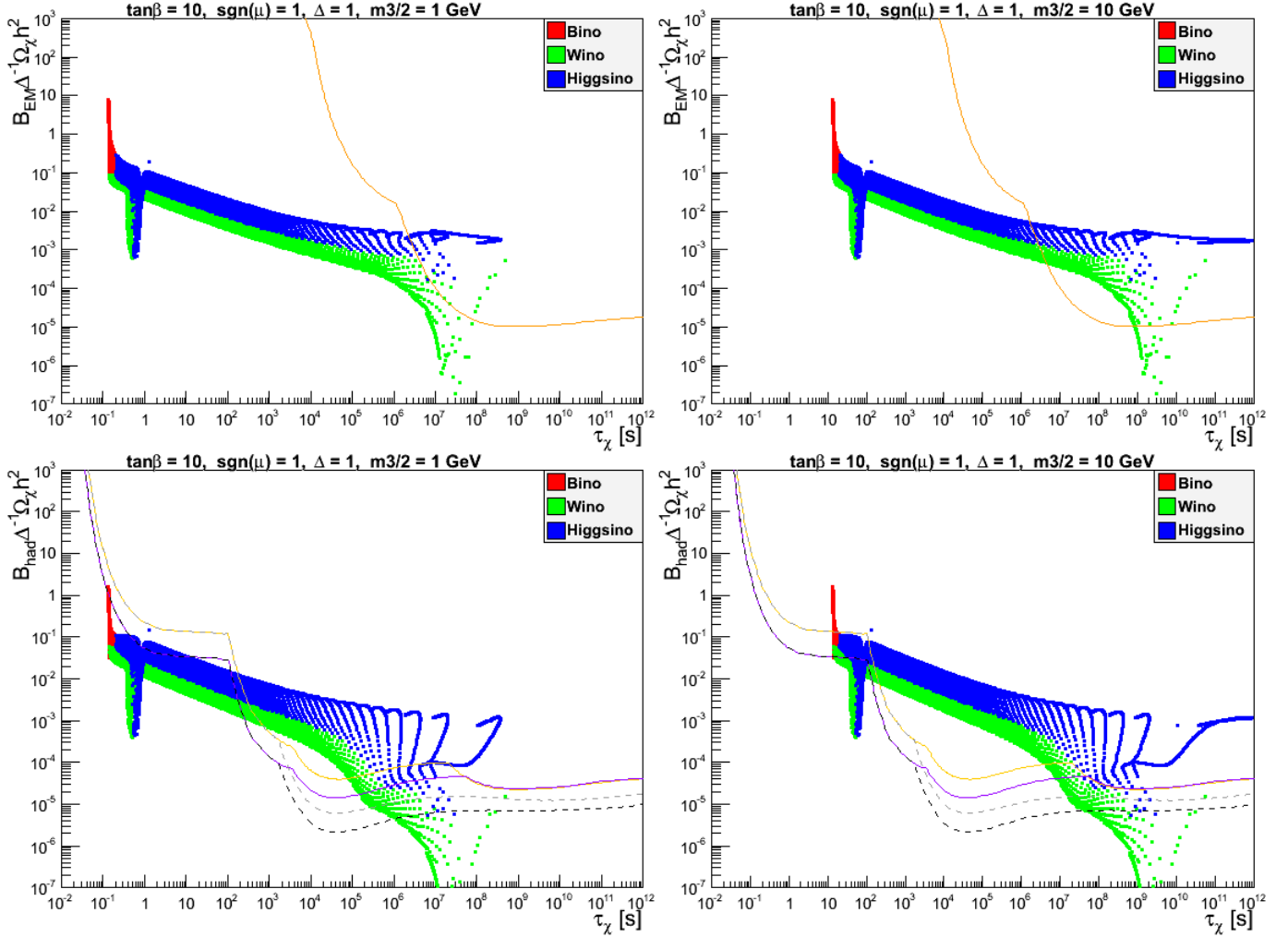
Figure 5.8: Relic density of wino-Higgsino NLSP compared to the BBN electromagnetic (top) and hadronic (bottom) constraints in the case of a 1 (left) and 10 (right) GeV gravitino LSP mass in the high energy scale. The continuous (dashed) lines corresponds to more (less) conservative bounds for the ^{6}Li to ^{7}Li ratio. The orange/upper and purple/lower lines correspond to constraints on a 1 TeV and 100 GeV decaying particle mass. The mass increases from right to left, and the composition goes from Higgsino at the top to wino at the bottom.
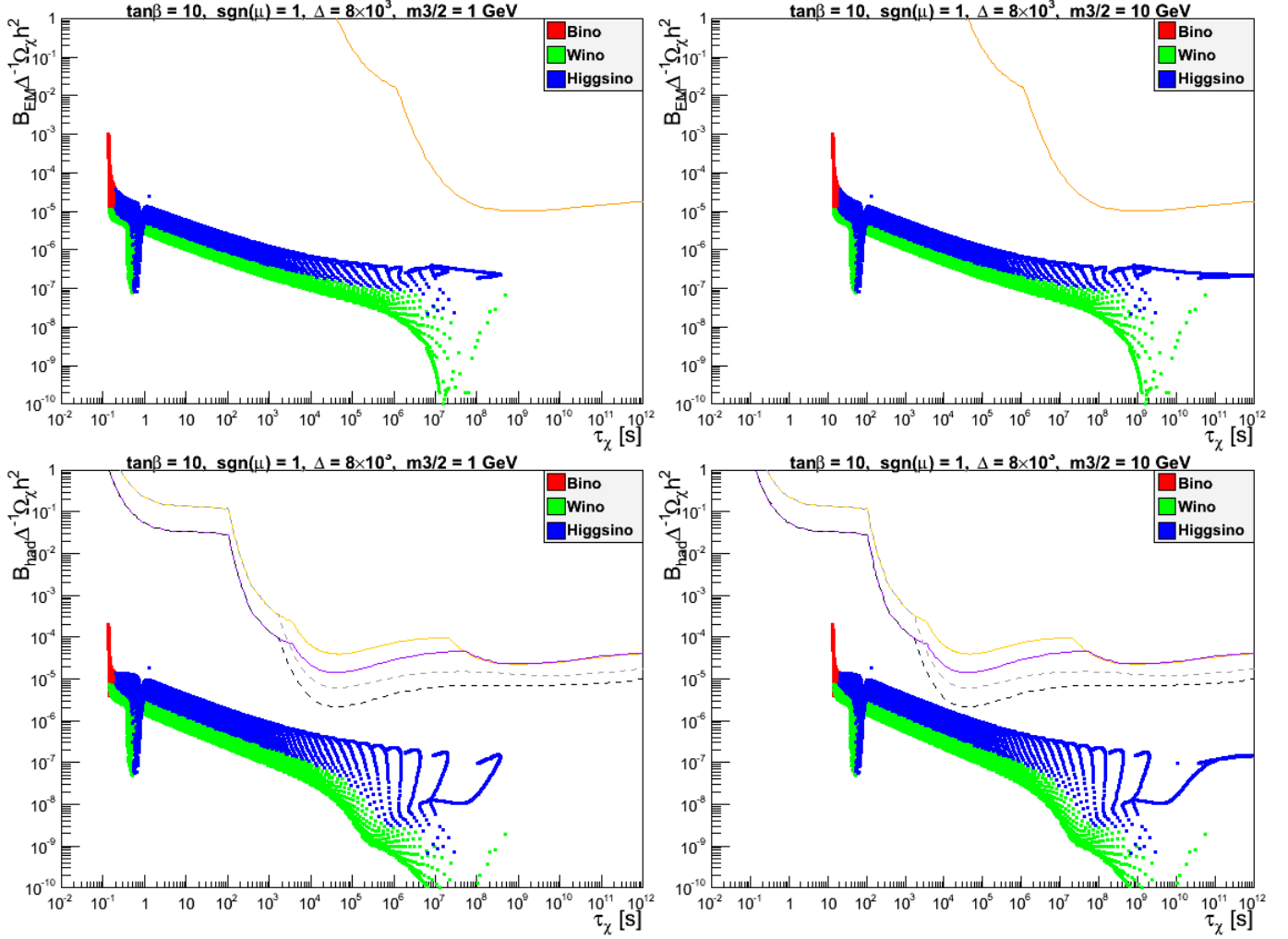
Figure 5.9: Relic density of wino-Higgsino NLSP compared to the BBN electromagnetic (top) and hadronic (bottom) constraints in the case of a 1 (left) and 10 (right) GeV gravitino LSP mass in the high energy scale for a non-unity Δ. The continuous (dashed) lines corresponds to more (less) conservative bounds for the ^{6}Li to ^{7}Li ratio. The orange/upper and purple/lower lines correspond to constraints on a 1 TeV and 100 GeV decaying particle mass. The mass increases from right to left, and the composition goes from Higgsino at the top to wino at the bottom.

Chapter 6

Conclusions

In this thesis we have considered gravitino dark matter with neutralino NLSP in the high energy scale, a non-unity dilution factor, and the implications from the constraints enforced by BBN.

In the graphs using the high energy scale parameters with a dilution factor equal to unity, we see that they are approximately equal to the low energy scale. After we introduced the non-unity dilution factor, the plots were more promising. We found that the bounds are much more relaxed, especially for wino- and Higgsino-dominated neutralinos, and thus it is possible to allow for much larger gravitino masses, $m_{3/2} \geq 100$ GeV, which is excellent news for thermal leptogenesis. The same is not true for the heavy bino case, as these points will move into the bounded region for higher gravitino mass.

Using the bound on the reheating temperature for thermal leptogenesis, $T_R \geq 1.5 \times 10^9$, we can rewrite (3.20) to show the reheating temperature as a function of the gravitino mass and the gluino mass

$$T_R \simeq 1.5 \times 10^9 \text{ GeV} \left(\frac{m_{3/2}}{100 \text{ GeV}} \right) \left(\frac{1.8 \text{ TeV}}{m_{\tilde{g}}} \right)^2 \qquad (6.1)$$

Here, we see that a higher gravitino mass is favoured, as this will push the upper bound for the gluino mass upwards to allow more massive gluinos while still satisfying the thermal leptogenesis bound. Our value for the gluino mass

parameter, $M_3 = 2.2$ TeV, will still agree with thermal leptogenesis if we assume a gravitino mass of $m_{3/2} \geq 150$ GeV.

We can interpret these results in two ways, depending on the initial amount of thermally produced gravitino dark matter acquired using (3.20). If we assume the thermal production to be $\Omega_{3/2} \simeq 0$, we detect some issues regarding the abundance of dark matter. Even though more of the parameter space and heavier gravitinos are allowed after we introduce a non-unity dilution factor, the resulting relic density from non-thermal production, $\Omega_{DM}^{\Delta} < 10^{-1}$, is too low to explain all the dark matter that we currently observe in the universe. Hence, a lower value for Δ is required. By interpolating the given plots, we see that an upper bound on the entropy production for a gravitino LSP neutralino NLSP model is required to be about $\Delta \lesssim 10^2$. However, this constraint will invalidate any gravitino mass larger than ~ 10 GeV. On the other hand, if we assume $\Omega_{3/2} > 0$, then the outlook is much brighter. The abundance of non-thermally produced dark matter is still too low, but in this case, we can adjust the reheating temperature such that the thermal production of dark matter ensures that the resulting dark matter density coincides with observational data. This is of course preferred if we want to allow for higher gravitino masses, while still abiding the BBN constraints.

Appendix A

Interfacing micrOMEGAs and making plots with ROOT

First, we started by making use of the default MSSM "main.cpp" file that shipped with micrOMEGAs. Within that file we disabled all the modules that were not used for calculating Ω, and inside the module that did, we added some lines to save the calculated Ω to a file. From there, we cloned the main file so that we had one for calculating the low energy case, and one for calculating the high energy case.

We needed the low energy main file as a control test so we could recreate the plots given in [16] (Figure 5.1, 5.4, 5.7 in this thesis), to make sure that the rest of the program ran as it was supposed to. In the low energy main file, we activated the "EWSB" module and used a micrOMEGAs custom ".par" parameter file as an input file to run the micrOMEGAs package. In the high energy main file, we activated the "SUGRANUH" module, and edited the module so we could use M_1, M_2, and μ as input parameters to run the micrOMEGAs package.

To use the micrOMEGAs main files we made, we wrote an interface that either ran the high energy case with the given parameters, or wrote a ".par" file to input to the low energy case depending on which case we were looking at. This interface class then read the output values from micrOMEGAs and returned them to the rest of our custom program. We could then use these values in our calculation class to calculate the lifetime and the hadronic

branching ratio from the equations given in Chapter 4. Then, we passed the calculated values on to the IO class which saved them to a file, in a format ROOT [20] could understand.

Our main program looped over the range of M_1, M_2, and μ, and used the process described above to obtain the lifetime and branching ratio for each instance in the parameter space. After the loops were finished, we ran the Graph class, to plot our data. This was done by using the "TMultiGraph" class in ROOT, which can plot multiple instances of "TGraph", and can therefore plot as many graphs in the same coordinate system as we like. We had one "TGraph" for each of the constraint lines, and one for each type of data point, i.e. one for bino-like points, one for wino-like points, and one for Higgsino-like points. These graphs were constructed by using the data files produced by the IO class directly as a parameter, and then inserted into the "TMultiGraph". Finally, we changed the labels and axes to our liking and then saved the plots to a file.

Appendix B

Calculating $\Gamma(\widetilde{G} \to \Psi_{3/2}Z)$

An example calculation of the width of a gaugino decaying into a gravitino and a Z-boson. The Feynman rules for this scenario are taken from [11] and given below. First, the vertex

$$= \frac{i}{4M_p}(-N_{11}c_W + N_{12}s_W)[\gamma^\rho, \slashed{p}_2]\gamma^\nu$$
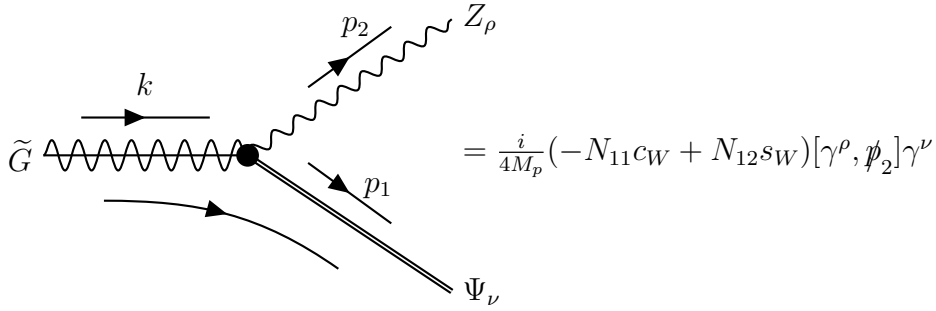
then, the following external lines

$$\Psi_\nu \to \bar{\psi}_\nu^{+r_1}(p_1)$$
$$Z_\rho \to \epsilon_\rho^{*r_2}(p_2)$$
$$\widetilde{G} \to u^s(k)$$

Using these rules, we can express the Feynman amplitude

$$\mathcal{M} = \frac{i}{4M_p}(-N_{11}s_W + N_{12}c_W)\bar{\psi}_\nu^{+r_1}(p_1)[\slashed{\epsilon}^{*r_2}(p_2), \slashed{p}_2]\gamma^\nu u^s(k)$$

where k, p_1, and p_2 are the momenta of the gaugino, gravitino, and Z boson respectively. Multiplying by the hermitian conjugate

$$\mathcal{M}^\dagger = -\frac{i}{4M_p}(-N_{11}s_W + N_{12}c_W)\bar{u}^s(k)\gamma^\mu[\slashed{p}_2, \slashed{\epsilon}^{r_2}(p_2)]\psi_\mu^{+r_1}(p_1)$$

and averaging over the polarizations, we obtain

$$
\begin{aligned}
|\mathcal{M}|^2_{\not{p}} =& \frac{1}{2} \sum_{s,r_1,r_2} \mathcal{M}^\dagger \mathcal{M} \\
=& -\frac{|-N_{11}s_W + N_{12}c_W|^2}{32M_p^2} \mathrm{Tr}(\Pi^+_{\mu\nu}(p_1)[\gamma_\sigma, \not{p}_2]\gamma^\nu(\not{k} + m_\chi)\gamma^\mu[\not{p}_2, \gamma^\sigma])
\end{aligned}
$$

by utilizing the following relations from [11]

$$
\sum_r u^r(p)\bar{u}^r(p) = \not{p} + m, \qquad \sum_r \psi^{+r}_\mu(p)\bar{\psi}^{+r}_\nu(p) = \Pi^+_{\mu\nu}(p),
$$

$$
\sum_r \epsilon^r_\mu(p)\epsilon^{*r}_\nu(p) = -g_{\mu\nu}
$$

where $\Pi^+_{\mu\nu}(p)$ is defined as

$$
\Pi^+_{\mu\nu}(p) = -(\not{p} + m)\left(g_{\mu\nu} - \frac{p_\mu p_\nu}{m^2}\right) - \frac{1}{3}\left(\gamma_\mu + \frac{p_\mu}{m}\right)(\not{p} - m)\left(\gamma_\nu + \frac{p_\nu}{m}\right)
$$

The above expression can be simplified to

$$
\begin{aligned}
|\mathcal{M}|^2_{\not{p}} =& -\frac{|-N_{11}s_W + N_{12}c_W|^2}{2M_p^2} p_{2\lambda}p_{2\kappa}\mathrm{Tr}(\Pi^+_{\mu\nu}(p_1)[k_\delta(2g^{\lambda\nu}g^{\mu\kappa}\gamma^\delta \\
& -2(g^{\kappa\nu}g^{\mu\delta} + g^{\mu\kappa}g^{\delta\nu})\gamma^\lambda + g^{\mu\nu}\gamma^\lambda\gamma^\delta\gamma^\kappa) + m_\chi\ g^{\mu\nu}\gamma^\lambda\gamma^\kappa])
\end{aligned}
$$

by using from [11] that

$$
\gamma^\mu\Pi_{\mu\nu} = 0, \qquad \Pi_{\mu\nu}\gamma^\nu = 0
$$

Evaluating the trace, we obtain

$$
\begin{aligned}
|\mathcal{M}|^2_{\not{p}} =& -\frac{|-N_{11}s_W + N_{12}c_W|^2}{32M_p^2}[-\frac{128}{3}(k \cdot p_1)p_2^2 + \frac{256}{3m_{3/2}^2}(k \cdot p_1)(p_1 \cdot p_2)^2 \\
& +\frac{256}{3}(k \cdot p_2)(p_1 \cdot p_2) + 128m_{3/2}m_\chi p_2^2]
\end{aligned}
$$

After inserting these relations from [11]

$$
k \cdot p_1 = \frac{1}{2}(m_\chi^2 + m_{3/2}^2 - m_Z^2) \qquad k \cdot p_2 = \frac{1}{2}(m_\chi^2 - m_{3/2}^2 + m_Z^2)
$$

$$
p_1 \cdot p_2 = \frac{1}{2}(m_\chi^2 - m_{3/2}^2 - m_Z^2)
$$

49

for the dot products, we arrive at the expression

$$
|\mathcal{M}|^2_{\not{P}} = -\frac{|-N_{11}s_W + N_{12}c_W|^2}{3M_p^2}\frac{m_\chi^6}{m_{3/2}^2}[(1 - x_{3/2}^2)^2(1 + 3x_{3/2}^2)
$$
$$
- x_Z^2\{3 + x_{3/2}^3(x_{3/2} - 12) - x_Z^2(3 - x_{3/2}^2 - x_Z^2)\}]
$$

where $x_i \equiv m_i/m_\chi$ is a convenient substitution. To calculate the width, we also have to find $|p_1|$, where the first equality is taken from [11]

$$
|p_1| = \frac{1}{2m_\chi}[(m_\chi^2 - (m_{3/2} + m_Z)^2)(m_\chi^2 - (m_{3/2} - m_Z)^2)]^{1/2}
$$
$$
= \frac{m_\chi}{2}(1 - 2(x_{3/2}^2 + x_Z^2) + (x_{3/2}^2 - x_Z^2)^2)^{1/2} \equiv \frac{m_\chi}{2}\beta_{\chi \to \Psi_{3/2}Z}
$$

From these expressions, we obtain the final width

$$
\Gamma(\widetilde{G} \to \Psi_{3/2}Z) = \frac{1}{8\pi}|\mathcal{M}|^2\frac{|p_1|}{m_\chi^2}
$$
$$
= \frac{|-N_{11}s_W + N_{12}c_W|^2}{48\pi M_p^2}\frac{m_\chi^5}{m_{3/2}^2}\beta_{\chi \to \Psi_{3/2}Z}[(1 - x_{3/2}^2)^2(1 + 3x_{3/2}^2)
$$
$$
- x_Z^2\{3 + x_{3/2}^3(x_{3/2} - 12) - x_Z^2(3 - x_{3/2}^2 - x_Z^2)\}]
$$

which is the same expression as given in [11].

Bibliography

[1] S.P. Martin, 2010. "A Supersymmetry Primer". *Adv. Ser. Direct. High Energy Phys*, 21(515), pp.1-153. arXiv:hep-ph/9709356.

[2] H. Iminniyaz, M. Drees, X. Chen, 2011. "Relic abundance of asymmetric dark matter". *Journal of Cosmology and Astroparticle Physics*, 2011(07), p.003. arXiv:1104.5548 [hep-ph].

[3] J. Hasenkamp, J. Kersten, 2010. "Leptogenesis, gravitino dark matter, and entropy production". *Physical Review D*, 82(11), p.115029. arXiv:1008.1740 [hep-ph].

[4] B.D. Fields, P. Molaro, S. Sarkar, 2014. "Big-bang nucleosynthesis". arXiv preprint arXiv:1412.1408 [astro-ph.CO].

[5] R.H. Cyburt, B.D. Fields, K.A. Olive, T.H. Yeh, 2016. "Big bang nucleosynthesis: Present status". *Reviews of Modern Physics*, 88(1), p.015004. arXiv:1505.01076 [astro-ph.CO].

[6] E.W. Kolb, M.S. Turner, 1990. "The Early Universe". ISBN 0-201-11603-0.

[7] K. Jedamzik, 2006. "Big bang nucleosynthesis constraints on hadronically and electromagnetically decaying relic neutral particles". *Physical Review D*, 74(10), p.103509. arXiv:hep-ph/0604251.

[8] S. Dimopoulos, D. Sutter, 1995. "The Supersymmetric flavor problem". *Nuclear Physics B*, 452(3), pp.496-512. arXiv:hep-ph/9504415.

[9] P. Bechtle, H.E. Haber, S. Heinemeyer, O. Stål, T. Stefaniak, G. Weiglein, L. Zeune, 2016. "The Light and Heavy Higgs Interpretation of the MSSM". arXiv preprint arXiv:1608.00638 [hep-ph].

[10] F.D. Steffen, 2006. "Gravitino dark matter and cosmological constraints". *Journal of Cosmology and Astroparticle Physics*, 2006(09), p.001. arXiv:hep-ph/0605306.

[11] J. Hasenkamp. "General neutralino NLSP with gravitino Dark Matter vs. Big Bang Nucleosynthesis", DESY-THESIS-2009-016.

[12] J. Edsjö, P. Gondolo, 1997. "Neutralino relic density including coannihilations". *Physical Review D*, 56(4), p.1879. arXiv:hep-ph/9704361.

[13] M. Bolz, A. Brandenburg, W. Buchmüller, 2001. "Thermal production of gravitinos". *Nuclear Physics B*, 606(1), pp.518-544. arXiv:hep-ph/0012052.

[14] G. Bertone, D. Hooper, J. Silk, 2005. "Particle dark matter: Evidence, candidates and constraints". *Physics Reports*, 405(5), pp.279-390. arXiv:hep-ph/0404175.

[15] G. Bertone, 2013. "Particle Dark Matter". ISBN 978-1-107-65392-4.

[16] L. Covi, J. Hasenkamp, S. Pokorski, J. Roberts, 2009. "Gravitino Dark Matter and general neutralino NLSP". *Journal of High Energy Physics*, 2009(11), p.003. arXiv:0908.3399 [hep-ph].

[17] G. Belanger, F. Boudjema, A. Pukhov, A. Semenov, 2014. "micrOMEGAs_3: A program for calculating dark matter observables". *Computer Physics Communications*, 185(3), pp.960-985. arXiv:1305.0237 [hep-ph].

[18] A. Djouadi, J.L. Kneur, G. Moultaka, 2007. "SuSpect: A Fortran code for the supersymmetric and Higgs particle spectrum in the MSSM".

Computer Physics Communications, 176(6), pp.426-455. arXiv:hep-ph/0211331.

[19] M. Breistein. "Late time entropy production in leptogenesis scenarios". Thesis, University of Bergen. To be submitted.

[20] I. Antcheva, M. Ballintijn, B. Bellenot, M. Biskup, R. Brun, N. Buncic, P. Canal, D. Casadei, O. Couet, V. Fine, L. Franco, G. Ganis, A. Gheata, D.G. Maline, M. Goto, J. Iwaszkiewicz, A. Kreshuk, D.M. Segura, R. Maunder, L. Moneta, A. Naumann, E. Offermann, V. Onuchin, S. Panacek, F. Rademakers, P. Russo, M. Tadel, 2009. "ROOT—A C++ framework for petabyte data storage, statistical analysis and visualization". *Computer Physics Communications*, 180(12), pp.2499-2512. arXiv:hep-ph/9704361.

Acknowledgements